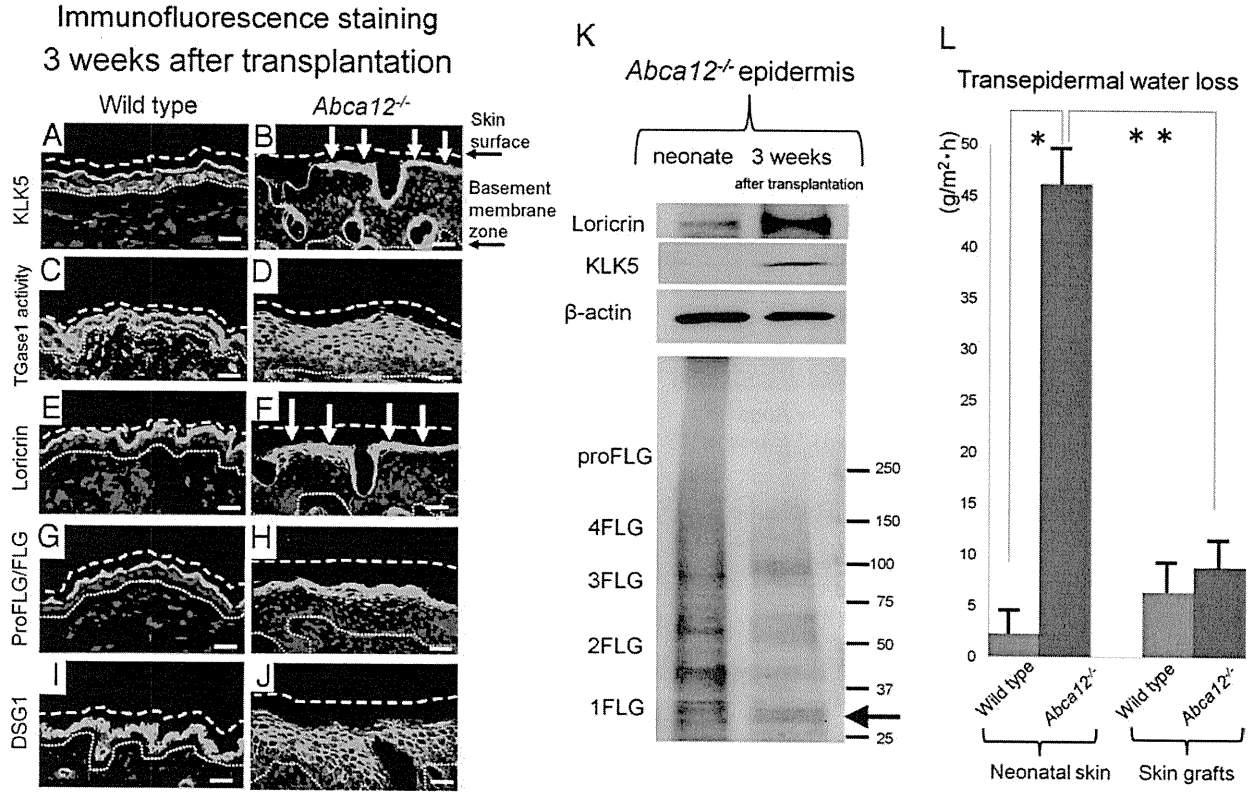

Figure 4. Improvement of previously disrupted differentiation-specific protein expression and defective skin barrier function in postnatal *Abca12*$^{-/-}$ skin. **A–J:** Immunolabeling for differentiation-specific molecules confirmed improved keratinization during maturation of the grafted *Abca12−/−* skin. Intense kallikrein 5 (KLK5) immunostaining (**A** and **B**, **white arrows**), *in situ* transglutaminase 1 (TGase1) activity labeling (**C** and **D**) and loricrin immunolabeling (**E** and **F**, **white arrows**) were seen throughout the granular layers in mature grafted *Abca12*$^{-/-}$ skin, compared with their sparse distribution in the *Abca12−/−* neonatal skin (see Figure 2, B, D and F). Increased loricrin and KLK5 immunolabeling intensity was confirmed by Western blot analysis using epidermal extracts from mature grafted *Abca12*$^{-/-}$ skin (**K**). Mature grafted *Abca12−/−* skin showed intense profilaggrin/filaggrin labeling in the granular layer (**H**), similar to the mature grafted wild-type skin (**G**). Diffuse profilaggrin/filaggrin staining in the entire cornified layers observed in *Abca12*$^{-/-}$ neonatal skin (see Figure 2H) disappeared in mature grafted *Abca12−/−* skin. Expression of desmoglein 1 (DSG1), unassociated with keratinization, was not altered in the grafted skin (**I** and **J**). Western blotting with anti-profilaggrin/filaggrin antibody revealed that normal conversion of profilaggrin to filaggrin was restored in mature *Abca12*$^{-/-}$ epidermis (**K**). Nuclear stain: propidium iodide, red; original magnification ×40; Scale bars = 20 μm. **L:** The barrier function in the transplanted skin was assessed by measuring transepidermal water loss (TEWL). The *Abca12−/−* neonates (red bar, left) showed significantly greater TEWL than the wild-type neonates (blue bar, left) showed ($^{*}P < 0.001$). TEWL levels of mature *Abca12*$^{-/-}$ epidermis three weeks after the skin graft (red bar, right) were significantly decreased as compared with levels of *Abca12−/−* neonatal skin (red bar, left) ($^{**}P < 0.001$), and was similar to levels of mature wild-type skin three weeks after the skin graft (blue bar, right). (*Abca12*$^{-/-}$ neonates, $n = 3$; wild-type neonates, $n = 3$; mature *Abca12−/−* skin, $n = 3$; mature wild-type skin, $n = 3$). KLK5, kallikrein 5; proFLG, profilaggrin; FLG, filaggrin; 4FLG, filaggrin tetramer; 3FLG, filaggrin trimer; 2FLG, filaggrin dimer; 1FLG, filaggrin monomer.

levels compared with primary-cultured *Abca12−/−* keratinocytes (Figure 5G). Blot extracts from differentiated primary-cultured *Abca12*$^{-/-}$ keratinocytes showed low expression of loricrin and KLK5 (Figure 5H), as observed in neonatal *Abca12−/−* mice epidermis (Figure 2L). However, extracts from subcultured *Abca12*$^{-/-}$ keratinocytes showed restoration of loricrin and KLK5 expression (Figure 5H), as observed in grafted mice epidermis (Figure 4K).

Western blotting with anti-profilaggrin/filaggrin antibody revealed that the filaggrin expression pattern had become normalized in subcultured *Abca12*$^{-/-}$ keratinocytes (Figure 5H). Cell lysates from10 passage-subcultured *Abca12−/−* keratinocytes showed an intense filaggrin monomer band that was faint in lysates from *Abca12*$^{-/-}$ primary first-passage keratinocytes.

Studies of subcultured *Abca12*$^{-/-}$ keratinocytes demonstrated restored differentiation, at least in part, similar to that observed in mature *Abca12−/−* skin grafts.

cDNA Microarray Analysis Revealed Up-Regulation of 22 Lipid Metabolic and/or Transport-Related Genes

To investigate the mechanism of restoration of intact keratinocytes differentiation in subcultured *Abca12*$^{-/-}$ keratinocytes, we analyzed whole gene expression profile of primary/subcultured *Abca12−/−* keratinocytes maintained under high Ca^{2+} condition using cDNA microarray methods. We obtained the 35,582 gene expression profile and observed 566 transcripts that were up-regulated more than three-fold in subcultured *Abca12−/−* keratinocytes compared with primary-cultured *Abca12*$^{-/-}$ keratinocytes. Among them, we searched for genes related to "lipid metabolism and/or lipid transporter function," and identified 22 specific transcripts including solute carrier family 22 member 7 (*Slc22a7*), prostaglandin D2 syn-

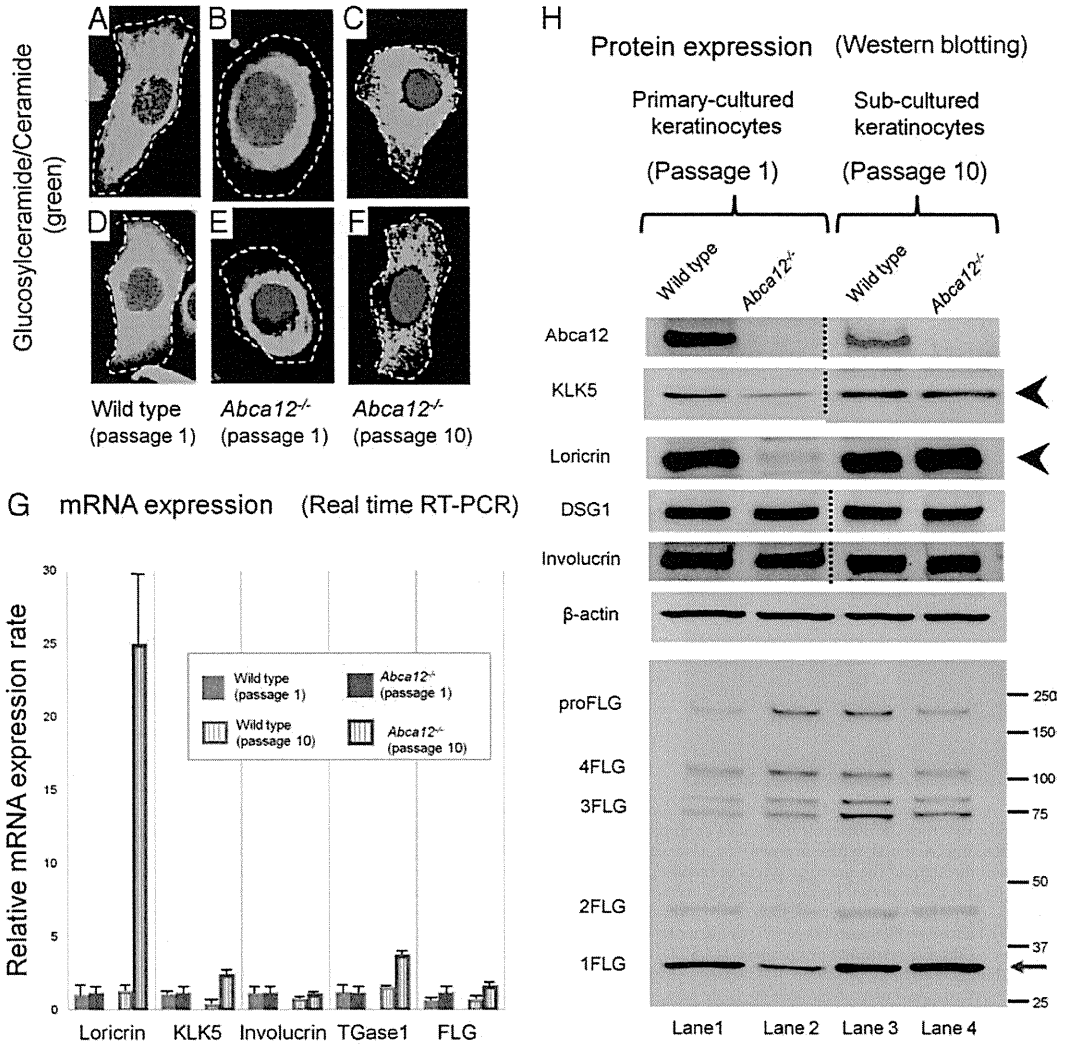

Figure 5. Subcultured *Abca12*$^{-/-}$ mouse keratinocytes exhibited restored intracytoplasmic localization of glucosylceramide/ceramide, protein expression of differentiation-specific molecules and profilaggrin conversion. **A–F:** Intracytoplasmic localization of glucosylceramide/ceramide in cultured keratinocytes. Immunolabeling demonstrated a congested pattern of glucosylceramide/ceramide (Alexa 488, green) in differentiated primary-cultured *Abca12−/−* mouse keratinocytes after first passage (**B** and **E**), in contrast with the uncongested, diffuse, peripheral pattern in the differentiated keratinocytes of a wild-type mouse (**A** and **D**). After 10 passages, subcultured *Abca12*$^{-/-}$ keratinocytes showed a widely distributed, diffuse glucosylceramide staining pattern (**C** and **F**), similar to those of wild-type keratinocytes. Subcultured wild-type keratinocytes after ten passages did not show any alterations in lipid distribution (data not shown). Nuclear stain: propidium iodide, red; original magnification ×60. **dotted lines** are the cell surface. **G:** There were no significant differences in loricrin, kallikrein 5 (KLK5), involucrin, transglutaminase 1 (TGase1), and filaggrin (FLG) mRNA expression between primary-cultured *Abca12−/−* keratinocytes (red bars, left) and primary-cultured wild-type keratinocytes (blue bars, left). Subcultured *Abca12*$^{-/-}$ keratinocytes (red bars, right) showed higher mRNA levels of loricrin, kallikrein 5, and transglutaminase 1 compared with primary-cultured *Abca12−/−* keratinocytes (red bars; left) and subcultured wild-type keratinocytes (blue bars, right). No significant difference was observed in involucrin and filaggrin mRNA expression. (primary-cultured *Abca12*$^{-/-}$, $n = 5$; primary-cultured wild-type, $n = 5$, subcultured *Abca12−/−*, $n = 5$; subcultured wild-type, $n = 5$, mRNA expression levels of *Abca12*$^{-/-}$ primary cultured keratinocytes = 1). **H:** Western blotting of differentiated cultured keratinocytes lysates under high Ca^{2+} condition showed that loricrin and KLK5 expression was lower in *Abca12−/−* primary-cultured keratinocytes (**lane 2**) than that of the wild-type primary-cultured keratinocytes (**lane 1**). Extracts from subcultured *Abca12*$^{-/-}$ keratinocytes showed restoration of loricrin and KLK5 expression (**lane 4**, **black arrowheads**). Western blotting with anti-profilaggrin/filaggrin antibody revealed that the *Abca12−/−* primary-cultured keratinocytes (**lane 2**) had reduced expression of mature filaggrin monomer than the wild-type primary-cultured keratinocytes (**lane 1**). In addition, the lysate from *Abca12*$^{-/-}$ primary-cultured keratinocytes exhibited plenty of high molecular weight bands, which indicated profilaggrin expression (**lane 2**). The filaggrin expression pattern was normalized in subcultured *Abca12−/−* keratinocytes (**lane 4**). Cell lysates from subcultured *Abca12*$^{-/-}$ keratinocytes showed an intense filaggrin monomer band that was faint in lysates from *Abca12−/−* primary first-passage keratinocytes (**lane 2** and **4**, **red arrow**). KLK5, kallikrein 5; TGase, transglutaminase; DSG1, desmoglein 1; proFLG, profilaggrin; 4FLG, filaggrin tetramer; 3FLG, filaggrin trimer; 2FLG, filaggrin dimer; 1FLG, filaggrin monomer.

thetase (*Ptgds*), annexin A9 (*Anxa9*), bactericidal/permeability-increasing protein-like 2 (*Bpil2*), phosphatidylethanolamine binding protein-2 variant 1 homolog (*Pbp2*), lipocalin 7 (*Tinagl*), *Gpr119*, solute carrier family 5 member 1 (*Slc5a1*), prostaglandin- endoperoxide synthase 2 (*Ptgs2*), and solute carrier family 30 member 1 (*Slc30a1*) (see Supplemental Table S1 at *http://ajp.amjpathol.org*). Notably, these genes included four ATP-binding transporter family members: *Abca17*, *Abca1a*, *Abcc5*, and *Abcb11* that were up-regulated at least three-fold.

Keratinocytes Treated with Retinoids Failed to Exhibit Normal Differentiation and Therapeutic Trials onto Grafted HI Model Mice Failed to Demonstrate Skin Phenotype Recovery

As treatment trials for primary keratinocytes, Western blotting revealed that primary-cultured wild-type keratinocytes expressed a large amount of loricrin peptide and had a decent amount of filaggrin monomer converted from profilaggrin (see Supplemental Figure S3 at *http://ajp.amjpathol.org*). Both isotretinoin (10^{-6} mol/L) and etretinate (10^{-6} mol/L) in the cultured medium for 48 hours lead to remarkable reduction of loricrin protein expression in primary-cultured wild-type keratinocytes, although filaggrin expression patterns were not altered. Neither isotretinoin (10^{-6} mol/L) nor etretinate (10^{-6} mol/L) improved the deficient loricrin protein expression or defective profilaggrin conversion in the primary-cultured *Abca12−/−* keratinocytes under high Ca^{2+} condition.

As a treatment trial for HI grafted skin, oral administration of various doses of isotretinoin (1 or 10 mg/kg daily for 10 consecutive days) to HI skin graft-recipient SCID mice demonstrated no change in the skin phenotype of grafted HI model mice skin at all (data not shown).

Discussion

Keratinocyte terminal differentiation (keratinization) is remarkably important to skin physiology and essential for epidermal function including barrier formation. Keratinization is a highly regulated process, involving a number of genes and pathways. Until now, abnormalities in keratinocyte differentiation have been reported in HI patients. Morphologically, Buxman et al[10] have reported that granular layers were absent or poorly formed in HI patient epidermis. Dale et al reported abnormal lamellar granules and defective profilaggrin conversion both in HI patients skin and their cultured keratinocytes.[11] Profilaggrin conversion to filaggrin is a key step during epidermal keratinization. Fleckman et al[12] reported that HI keratinocytes in 3 dimensional culture were unable to show the adequate differentiated epithelium and profilaggrin/filaggrin conversion. Recently, Thomas et al reported that the desquamation specific enzyme, kallikrein 5, and cathepsin D, were remarkably reduced in HI model skin using ABCA12 small interfering RNA knockdown keratinocytes.[13]

In the present study, we have demonstrated that keratinocyte differentiation was severely disrupted in both *Abca12*$^{-/-}$ HI neonatal model mouse skin and primary-cultured *Abca12−/−* keratinocytes. The present findings were consistent with previous reports of findings in HI patient's skin. Our neonatal HI model mice skin showed no apparent keratohyalin granules within any of their granular layer cells, which was consistent with Buxman's study.[10] Furthermore, our immunoblotting results confirmed defective profilaggrin/filaggrin conversion, which was consistent with the studies by Dale et al[11] and Fleckman et al.[12] Our immunostaining and immunoblotting results showed reduced expression of KLK5 in neonatal *Abca12*$^{-/-}$epidermis and primary-cultured *Abca12−/−* keratinocytes, which was consistent with the study by Thomas et al.[13] We therefore believe that our *Abca12*$^{-/-}$ HI model mouse faithfully reproduces the molecular condition thus far identified in human HI epidermis in addition to mimicking clinical phenotype.[5]

Zuo et al[6] suggested that loss of ABCA12 did not induce a block in the normal processing of profilaggrin to filaggrin in another reported ABCA12 deficient mouse strain, although the solubility of filaggrin was altered. We believe that our data are consistent with Zuo's study. In the present study, we showed high molecular weight bands in RIPA buffer extracted supernatant from neonatal *Abca12*$^{-/-}$epidermis. In study by Zuo et al,[6] similar high molecular weight bands were also seen by the Western blotting after detergent buffer supernatant extraction. We also showed an alteration in filaggrin monomer solubility using 8 mol/L urea supernatant, reproducing the findings of Zuo et al.[6] The major difference between these two studies is that Zuo et al[6] showed no filaggrin monomer band after detergent buffer supernatant extraction in their ABCA12 deficient mouse skin. In contrast, we detected filaggrin monomer band in RIPA supernatant of our *Abca12−/−*neonatal epidermis. This finding might result from differences in lysis buffer, tissue sample

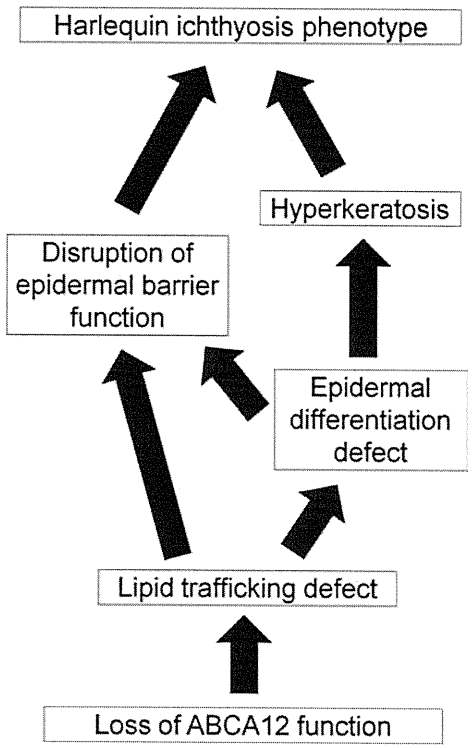

Figure 6. Putative pathomechanism of harlequin ichthyosis. Based on our results, we propose a novel pathogenetic mechanism underlying harlequin ichthyosis (HI). Our results suggested that a lipid trafficking defect due to loss of ABCA12 function leads to not only malformation of the epidermal lipid barrier but also "an epidermal differentiation defect." In our hypothesis, the severe hyperkeratosis, a characteristic phenotype of HI skin, is not a hyperkeratosis compensating for any barrier insufficiency, but a hyperkeratosis due to both defective differentiation and an abnormal desquamation process. The present scenario explains both the HI skin phenotype at/after birth and even *in utero*.

(whole skin or only epidermis), or harvest time (E18.5 or neonate). We conclude that neonatal *Abca12*$^{-/-}$ epidermis exhibits not only defective profilaggrin/filaggrin conversion but also alterations in filaggrin monomer solubility, as previously suggested by Dale et al,[11] Fleckman et al,[12] and Zuo et al.[6]

Based on our results, we propose several new pathogenetic mechanisms for HI (Figure 6). Our results suggest that "an epidermal differentiation defect" is the major pathomechanism in HI. This new pathogenesis model is furthermore able to resolve the conflicting "the barrier insufficiency" theory with the (human) HI clinical phenotype. Our novel "epidermal differentiation" theory can explain HI skin phenotype at birth and even *in utero*. In our theory, severe hyperkeratosis, characteristic of the HI skin phenotype, was not a compensative hyperkeratosis for barrier insufficiency, but a hyperkeratosis due to defective differentiation and desquamation processes.

Epidermal differentiation defects in our HI model mice suggest that ABCA12 lipid trafficking, which occurs during the early stages of keratinization, is a crucial step for correct keratinocyte terminal differentiation. In normal granular layer keratinocytes, ABCA12 transports lipids and forms lamellar granules.[3] Just after the extrusion of lipids from lamellar granules at the granular/cornified layer interface, loricrin accumulates at the cell periphery and is integrated into the insoluble cornified cell envelope by transglutaminases.[14] At the final phase of terminal differentiation, profilaggrin undergoes many post-translational modifications, including conversion to functional filaggrin monomers, which aid in the bundling of keratin intermediate filaments and formation of the cornified cell envelope.[14–16] Serine proteases including KLK5 are involved in the desquamation process after keratinization.[17] Our present results suggest that defective lipid trafficking and lamellar granule formation fail to initiate the normal sequence of events of the keratinization process. These facts indicate that ABCA12 lipid trafficking is essential to precisely regulate keratinocyte differentiation.

Interestingly, mature grafted HI model mouse skin and subcultured *Abca12*$^{-/-}$ keratinocytes showed improvement in the *Abca12−/−*-related abnormalities observed in neonatal skin and primary-cultured keratinocytes, such as the aberrant ceramide distribution, reduced differentiation-specific protein expression and profilaggrin/filaggrin conversion defects. Similar to our *Abca12*$^{-/-}$ model mouse skin, improvement in skin manifestations during maturation was observed in several other ichthyotic model mice. Loricrin knockout mice exhibit shiny translucent skin at birth although these mice showed a normal skin phenotype at 4 to 5 days after birth.[18] Biochemically, the mice showed increased protein expression of small proline rich proteins, which are also cornified cell envelope components during skin maturation.[18] Mature 12R-lipoxygenase knockout mouse skin showed recovery of skin barrier function and restoration of profilaggrin conversion after maturation, which had been lacking in the neonatal mice.[19,20] In addition, mature transglutaminase 1 knockout mouse skin also showed skin barrier functional recovery, although exact compensation mechanisms other than hyperkeratosis were not identified.[21]

To find any clues for the mechanism of compensation in *Abca12*$^{-/-}$ mice, we conducted cDNA microarray analysis. We could find that several transporters including four ATP-binding cassette (ABC) transporter family genes were up-regulated in subculture compared with primary-cultured *Abca12−/−* keratinocytes. We consider these up-regulated ABC transporters as prime candidate genes to compensate for the loss of ABCA12 function. These lipid transport/metabolism-related molecules might help in lipid trafficking and/or recovery of epidermal differentiation in *Abca12*$^{-/-}$ keratinocytes.

The recovery of skin barrier function and self-improvement of epidermal differentiation defects in mature *Abca12*$^{-/-}$ skin gave us important clues to aid in treatment of HI patients. Infants affected with HI frequently die within the neonatal period, although the survival rate of HI newborns has increased recently with the arrival of neonatal intensive care regimes with retinoid administration.[22–26] Our observations in mature *Abca12−/−* skin further confirmed that the early neonatal period is a critical time defining the prognosis. In this context, neonatal intensive care for HI newborns in the initial neonatal period is important for their survival.

We had already tried systemic retinoid administration to pregnant mice as a fetal therapy, although neither improvement of the skin manifestations nor extension of the survival period was obtained in the *Abca12*$^{-/-}$ newborns from the treated-mother mice.[5] Based on the clinical efficacy of retinoids to HI patients,[22–26] we conducted retinoid administration to the primary-cultured *Abca12−/−* keratinocytes. We could not detect any recovery of differentiation defects in the primary-cultured *Abca12*$^{-/-}$ keratinocytes treated with retinoids. These results of our therapeutic trials to fetuses in the previous report[5] and to primary keratinocytes in this study indicated that retinoids may be ineffective for modifying the epidermal differentiation defects during the fetal period. These facts were consistent with the known effects of retinoids, which enhance proliferation and suppress differentiation of keratinocytes.[27,28] Further, we performed a treatment trial on grafted SCID mice using systemic isotretinoin administration. Oral administration of any dose of isotretinoin (either 1 or 10 mg/kg daily, for 10 consecutive days) to the HI-skin-grafted SCID mice failed to improve the skin phenotype of grafted HI skin at all. We failed to obtain any clue to understand the reason why retinoids are only effective for HI patients from our present study.

In conclusion, we have demonstrated that disrupted epidermal keratinocyte differentiation is the pathomechanism involved in HI, and that during maturation, *Abca12*$^{-/-}$ epidermal keratinocytes regain normal keratinocyte differentiation. This restoration of differentiation is likely to be associated with the skin phenotype improvement observed in HI survivors.

Acknowledgment

We thank Dr. James R. McMillan for proofreading this manuscript.

References

1. Akiyama M: Pathomechanisms of harlequin ichthyosis and ABCA transporters in human diseases. Arch Dermatol 2006, 142:914–918
2. Hovnanian A: Harlequin ichthyosis unmasked: a defect of lipid transport. J Clin Invest 2005, 115:1708–1710
3. Akiyama M, Sugiyama-Nakagiri Y, Sakai K, McMillan JR, Goto M, Arita K, Tsuji-Abe Y, Tabata N, Matsuoka K, Sasaki R, Sawamura D, Shimizu H: Mutations in lipid transporter ABCA12 in harlequin ichthyosis and functional recovery by corrective gene transfer. J Clin Invest 2005, 115:1777–1784
4. Kelsell DP, Norgett EE, Unsworth H, Teh MT, Cullup T, Mein CA, Dopping-Hepenstal PJ, Dale BA, Tadini G, Fleckman P, Stephens KG, Sybert VP, Mallory SB, North BV, Witt DR, Sprecher E, Taylor AE, Ilchyshyn A, Kennedy CT, Goodyear H, Moss C, Paige D, Harper JI, Young BD, Leigh IM, Eady RA, O'Toole EA: Mutations in ABCA12 underlie the severe congenital skin disease harlequin ichthyosis. Am J Hum Genet 2005, 76:794–803
5. Yanagi T, Akiyama M, Nishihara H, Sakai K, Nishie W, Tanaka S, Shimizu H: Harlequin ichthyosis model mouse reveals alveolar collapse and severe fetal skin barrier defects. Hum Mol Genet 2008, 17:3075–3083
6. Zuo Y, Zhuang DZ, Han R, Isaac G, Tobin JJ, McKee M, Welti R, Brissette JL, Fitzgerald ML, Freeman MW: ABCA12 maintains the epidermal lipid permeability barrier by facilitating formation of ceramide linoleic esters. J Biol Chem 2008, 283:36624–36635
7. Akiyama M, Smith LT, Shimizu H: Expression of transglutaminase activity in developing human epidermis. Br J Dermatol 2000, 142:223–225
8. Raghunath M, Hennies HC, Velten F, Wiebe V, Steinert PM, Reis A, Traupe H: A novel in situ method for the detection of deficient transglutaminase activity in the skin. Arch Dermatol Res 1998, 290: 621–627
9. Masukawa Y, Narita H, Shimizu E, Kondo N, Sugai Y, Oba T, Homma R, Ishikawa J, Takagi Y, Kitahara T, Takema Y, Kita K: Characterization of overall ceramide species in human stratum corneum. J Lipid Res 2008, 49:1466–1476
10. Buxman MM, Goodkin PE, Fahrenbach WH, Dimond RL: Harlequin ichthyosis with epidermal lipid abnormality. Arch Dermatol 1979, 115:189–193
11. Dale BA, Holbrook KA, Fleckman P, Kimball JR, Brumbaugh S, Sybert VP: Heterogeneity in harlequin ichthyosis, an inborn error of epidermal keratinization: variable morphology and structural protein expression and a defect in lamellar granules. J Invest Dermatol 1990, 94:6–18
12. Fleckman P, Hager B, Dale BA: Harlequin ichthyosis keratinocytes in lifted culture differentiate poorly by morphologic and biochemical criteria. J Invest Dermatol 1997, 109:36–38
13. Thomas AC, Tattersall D, Norgett EE, O'Toole EA, Kelsell DP: Premature terminal differentiation and a reduction in specific proteases associated with loss of ABCA12 in Harlequin ichthyosis. Am J Pathol 2009, 174:970–978
14. Bickenbach JR, Greer JM, Bundman DS, Rothnagel JA, Roop DR: Loricrin expression is coordinated with other epidermal proteins and the appearance of lipid lamellar granules in development. J Invest Dermatol 1995, 104:405–410
15. Candi E, Schmidt R, Melino G: The cornified envelope: a model of cell death in the skin. Nat Rev Mol Cell Biol 2005, 6:328–340
16. Denecker G, Ovaere P, Vandenabeele P, Declercq W: Caspase-14 reveals its secrets. J Cell Biol 2008, 180:451–458
17. Meyer-Hoffert U, Wu Z, Schroder JM: Identification of lympho-epithelial Kazal-type inhibitor 2 in human skin as a kallikrein-related peptidase 5-specific protease inhibitor. PLoS One 2009, 4:e4372
18. Koch PJ, de Viragh PA, Scharer E, Bundman D, Longley MA, Bickenbach J, Kawachi Y, Suga Y, Zhou Z, Huber M, Hohl D, Kartasova T, Jarnik M, Steven AC, Roop DR: Lessons from loricrin-deficient mice: compensatory mechanisms maintaining skin barrier function in the absence of a major cornified envelope protein. J Cell Biol 2000, 151:389–400
19. Epp N, Furstenberger G, Muller K, de Juanes S, Leitges M, Hausser I, Thieme F, Liebisch G, Schmitz G, Krieg P: 12R-lipoxygenase deficiency disrupts epidermal barrier function. J Cell Biol 2007, 177: 173–182
20. de Juanes S, Epp N, Latzko S, Neumann M, Furstenberger G, Hausser I, Stark HJ, Krieg P: Development of an Ichthyosiform Phenotype in Alox12b-Deficient Mouse Skin Transplants. J Invest Dermatol 2009, 129:1429–1436
21. Kuramoto N, Takizawa T, Takizawa T, Matsuki M, Morioka H, Robinson JM, Yamanishi K: Development of ichthyosiform skin compensates for defective permeability barrier function in mice lacking transglutaminase 1. J Clin Invest 2002, 109:243–250
22. Prasad RS, Pejaver RK, Hassan A, Dusari S, Wooldridge MA: Management and follow-up of harlequin siblings. Br J Dermatol 1994, 130:650–653
23. Lawlor F, Peiris S: Harlequin fetus successfully treated with etretinate. Br J Dermatol 1985, 112:585–590
24. Ward PS, Jones RD: Successful treatment of a harlequin fetus. Arch Dis Child 1989, 64:1309–1311
25. Haftek M, Cambazard F, Dhouailly D, Reano A, Simon M, Lachaux A, Serre G, Claudy A, Schmitt D: A longitudinal study of a harlequin infant presenting clinically as non-bullous congenital ichthyosiform erythroderma. Br J Dermatol 1996, 135:448–453
26. Singh S, Bhura M, Maheshwari A, Kumar A, Singh CP, Pandey SS: Successful treatment of harlequin ichthyosis with acitretin. Int J Dermatol 2001, 40:472–473
27. Eichner R, Kahn M, Capetola RJ, Gendimenico GJ, Mezick JA: Effects of topical retinoids on cytoskeletal proteins: implications for retinoid effects on epidermal differentiation. J Invest Dermatol 1992, 98:154–161
28. Eichner R: Epidermal effects of retinoids: in vitro studies. J Am Acad Dermatol 1986, 15:789–797

The American Journal of Pathology, Vol. 176, No. 2, February 2010

DOI: 10.2353/ajpath.2010.090744

Stem Cells, Tissue Engineering and Hematopoietic Elements

Blockade of Autoantibody-Initiated Tissue Damage by Using Recombinant Fab Antibody Fragments against Pathogenic Autoantigen

Gang Wang,*† Hideyuki Ujiie,* Akihiko Shibaki,* Wataru Nishie,* Yasuki Tateishi,* Kazuhiro Kikuchi,* Qiang Li,* James R. McMillan,*† Hiroshi Morioka,‡ Daisuke Sawamura,* Hideki Nakamura,* and Hiroshi Shimizu*

From the Department of Dermatology, Hokkaido University Graduate School of Medicine, the Creative Research Initiative Sousei,† and the Faculty of Pharmaceutical Sciences,‡ Hokkaido University, Sapporo, Japan*

Activation of the complement cascade via the classical pathway is required for the development of tissue injury in many autoantibody-mediated diseases. It therefore makes sense to block the pathological action of autoantibodies by preventing complement activation through inhibition of autoantibody binding to the corresponding pathogenic autoantigen using targeted Fab antibody fragments. To achieve this, we use bullous pemphigoid (BP) as an example of a typical autoimmune disease. Recombinant Fabs against the non-collagenous 16th-A domain of type XVII collagen, the main pathogenic epitope for autoantibodies in BP, were generated from antibody repertoires of BP patients by phage display. Two Fabs, Fab-B4 and Fab-19, showed marked ability to inhibit the binding of BP autoantibodies and subsequent complement activation *in vitro*. In the *in vivo* experiments using type XVII collagen humanized BP model mice, these Fabs protected mice against BP autoantibody-induced blistering disease. Thus, the blocking of pathogenic epitopes using engineered Fabs appears to demonstrate efficacy and may lead to disease-specific treatments for antibody-mediated autoimmune diseases. *(Am J Pathol 2010, 176:914–925; DOI: 10.2353/ajpath.2010.090744)*

Autoimmune diseases are a major cause of morbidity and mortality in humans, affecting approximately 5% of the general population.[1] In recent years, significant advances have been made in our understanding of autoimmune disease pathomechanisms, especially the roles of autoantibodies, complement system, and autoresponsive T cells. For many autoimmune diseases such as systemic lupus erythematosus, rheumatoid arthritis, anti-phospholipid syndrome (APS), and bullous pemphigoid (BP), complement activation is increasingly recognized as critical to tissue injury.[2–6] Studies of APS and BP, for example, showed that the classical pathway of complement activation is required for the development of tissue injury, although alternative pathways may also be involved.[4,7–9]

BP is the most common autoimmune blistering skin disease. Autoantibodies against collagen XVII (COL17) bind to dermal–epidermal junction (DEJ) components and activate the complement system that mediates a series of inflammatory events including dermal mast cell degranulation and generation of eosinophil-rich infiltrates, resulting in skin blister formation.[10–12] APS is a condition characterized by recurrent miscarriage and thrombosis formation in the presence of anti-phospholipid autoantibodies, and a therapy has been proven effective to prevent the fetal loss by using heparin to inhibit anti-phospholipid antibody–induced complement activation.[7,13,14] In both BP and APS, $F(ab')_2$ fragments from the pathogenic autoantibodies, which lack the Fc portion necessary to activate the complement pathway, fail to initiate the disease.[4,7] This suggests that preventing complement activation by blocking the binding of autoantibodies to the corresponding antigens can be a viable novel therapeutic strategy for treating these diseases.

Supported by a grant-in-aid from the Program for Promotion of Fundamental Studies in Health Sciences of the National Institute of Biomedical Innovation (NIBIO; to H.S.).

G.W. and H.U. contributed equally to this work. A.S. and H.S. contributed equally to the direction of this study.

Accepted for publication October 7, 2009.

Supplemental material for this article can be found on *http://ajp.amjpathol.org*.

Address reprint requests to Dr. Akihiko Shibaki or Dr. Hiroshi Shimizu, Department of Dermatology, Hokkaido University Graduate School of Medicine, N15 W7, Sapporo, 060-8638 Japan. E-mail: ashibaki@med.hokudai.ac.jp or shimizu@med.hokudai.ac.jp.

Table 1. PCR Primers for the Amplification of Human Antibody Gene Repertoires

Primers for κ	
HK5	5′-GAMATYGAGCTCACSCAGTCTCCA-3′ (Sac I)
HK3	5′-GCGCCGTCTAGAACTAACACTCTCCCCTGTTGAAGCTCTTTGTGACGGGCAAG-3′ (Xba I)
Primers for λ	
HL5	5′-CASTYTGAGCTCACKCARCCGCCCTC-3′ (Sac I)
HL3	5′-GAGGGATCTAGAATTATGAACATTCTGTAGG-3′ (Xba I)
Primers for Fd	
H135	5′-CAGGTGCAGCTGGTGSAGTCTGG-3′
H2	5′-CAGGTCAACTTGAAGGAGTCTGG-3′
H4	5′-CAGGTGCAGCTGCAGGAGTCGGG-3′
VH5	5′-CAGGTGCAGCTCGAGSAGTCTGG-3′ (Xho I)
HG3	5′-GCATGTACTAGTTTTGTCACAAGA-3′ (Spe I)

To allow for sequence variability, representative choices of wobble nucleotides were included in the primers (M = A/C, K = G/T, R = A/G, S = C/G, Y = C/T). Fd fragments of human IgG were amplified in a two-step procedure. First, antisense primers H135, H2, and H4 were combined with HG3 for the amplification of heavy chain genes from human VH1–VH5 families and the *Spe* I site was introduced. In the second step, antisense primer VH5 was combined with HG3 to reamplify the heavy chain genes and introduce the *Xho* I site. Underlined sequences are restriction sites for the enzymes indicated in parenthesis.

The purpose of this study is to provide a proof of concept for this new strategy of treating antibody-mediated autoimmune disorders by using recombinant Fabs to block complement activation induced by pathogenic autoantibodies. Toward this end, we use BP as an example of a typical autoimmune disease. Our group has recently established a BP mouse model using a newly constructed COL17 humanized mouse.[3] Here we report our success in developing Fabs against the noncollagenous 16th-A domain (NC16A) of COL17, the main pathogenic epitope of BP autoantibodies,[15] for the blockade of autoantibody-initiated BP disease.

Materials and Methods

Construction of Phage Antibody Libraries

We constructed two individual Fab phage libraries from mononuclear cells isolated from two patients with active BP. The diagnosis of BP was made by the typical clinical and histological manifestations as well as by laboratory data including anti-COL17 ELISA and indirect immunofluorescence (IIF). Phagemid expression vector p3MH, a gift from Dr. Yan Wang (Central Lab of Navy General Hospital, Beijing, China), was derived from pCOMB3H (Scripps Research Institute, La Jolla, CA) by adding 9E10/c-*myc* epitope for detection and a hexahistidine tag for column purification at the 3′ end of Fd.[16] Using previously described methods and a set of PCR primers (Table 1),[17–19] antibody genes were amplified by RT-PCR from approximately 1×10^8 mononuclear cells isolated from 50 ml of peripheral blood from each patient. The phage antibody libraries were constructed by randomly combining the genes coding Fd fragments of IgG heavy chains with IgG light chain genes of either lambda or kappa DNA in equal amounts (see Supplemental Figure S1 at http://ajp.amjpathol.org.). The phagemid libraries were electroporated into *E. coli* XL1-Blue strain (Stratagene, La Jolla, CA), and the phage display of the libraries was performed as described elsewhere.[17,20] Before amplification, the resulting libraries were examined for the coexpression of heavy and light chains by enzyme digestion and for the diversity by fingerprinting of antibody genes (Fd and light chain) of 24 randomly selected single colonies.[20,21] The amplified recombinant phages were purified from culture supernatants by polyethylene glycol precipitation and resuspended in PBS, pH 7.4, containing 1% bovine serum albumin (BSA) and 10% glycerol.

Isolation of Phage Antibodies against NC16A Domain of Human COL17

Recombinant fusion peptide of the human COL17 NC16A domain (rhNC16A) with glutathione S-transferase (GST) was synthesized as reported previously.[3] Library panning was performed routinely.[20–22] Briefly, a freshly amplified phage library (approximately 1×10^{12} phages) was incubated for 2 hours at 37°C in immuno-tubes (Nunc, Roskilde, Denmark) coated with 50 μg/ml rhNC16A in 50 mmol/L $NaHCO_3$ pH 9.6. After washing of the tube with 0.05% (v/v) Tween-20 in PBS, adherent phages were eluted with 0.1 mol/L triethylamine (Sigma-Aldrich, Inc., St. Louis, MO). After neutralization with 1 mol/L Tris, pH 7.4, eluted phages were used to infect a fresh culture of XL1-Blue *E. coli*, which was amplified overnight as previously described.[20] Phages were harvested from culture supernatants and then repanned against rhNC16A for three subsequent rounds as described for the original library. Individual single ampicillin-resistant colonies resulting from infection of *E. coli* XL1-Blue with the eluted phage from the fourth panning round were isolated, and the binding to rhNC16A was confirmed by ELISA using HRP-conjugated anti-M13 mAb (Amersham Biosciences UK Ltd., Little Chalfont, Buckinghamshire, UK) as the developing reagent. The specific binders were screened by gene fingerprinting and sequencing to identify different clones. The variable region sequences of the separate selected clones were analyzed for homology to known human V, D, and J genes using the V BASE database (http://vbase.mrc-cpe.cam.ac.uk/).

Production, Purification, and Characterization of Soluble Fab

Fab Production and Purification

Plasmid DNA of the distinct selected clones was prepared, digested by *Nhel* (New England BioLabs,

Ipswich, MA) to remove the gene III fragment, self ligated, and transformed into *E. coli* XL1-Blue. Clones were grown in LB containing 100 μg/ml ampicillin, and Fab expression was induced using 1 mmol/L isopropyl β-D-thiogalactopyranoside (IPTG, Sigma) in culture grown at 30°C overnight. Cells were pelleted by centrifugation, and the supernatant containing soluble Fab was taken for analysis.

Large-scale production of Fabs was achieved by growing Fab-express clones in *E. coli* XL1-Blue in 1 L of LB (plus 100 μg/ml ampicillin). Protein production was then induced with 1 mmol/L IPTG by culturing overnight at 30°C at 240 rpm. The culture supernatant was harvested by centrifugation. Fab purification was performed using HisTrap FF crude column (GE Healthcare Bio-Sciences AB, Uppsala, Sweden) according to the manufacturer's instructions. The purified Fabs were dialyzed against PBS and concentrated by Amicon ultrafiltration (Millipore, Lexington, MA) and were then characterized by SDS-PAGE and Western blotting. For animal experiments, the concentration of endotoxin in the purified Fabs was detected with the limulus amoebocyte lysate test using the QCL-1000 kit (Cambrex Bio Science Walkersville, Inc., Walkersville, MD), and endotoxin removal was performed by using Detoxi-Gel AffinityPak column (Pierce, Rockford, IL), where necessary.

ELISA

The binding activity and specificity of Fabs was confirmed by ELISA assay. ELISA plate wells were coated with 5 μg/ml rhNC16A in 50 mmol/L $NaHCO_3$ pH 9.6. Recombinant mouse NC16A (rmNC16A), GST, and BSA were used as negative control antigens at similar concentrations. Supernatant containing Fabs or appropriately diluted purified Fabs was incubated on ELISA plates. After washing, plates were developed with HRP-conjugated mAbs to human lambda light chain (Kirkegaard & Perry Laboratories, Gaithersburg, MD) or kappa light chain (Bethyl Laboratories, Inc., Montgomery, TX) and o-phenylenediamine substrate (Wako, Osaka, Japan). Absorbance was read at 492 nm.

Western Blotting

Western blotting was performed as previously described. Briefly, recombinant proteins were electrophoresed on SDS-PAGE and electrotransferred onto nitrocellulose membrane. The blots were blocked with 5% milk in TBS/T and incubated for 1 hour with the diluted Fabs at room temperature. After washing, the blots were incubated with HRP-conjugated mAbs to human lambda light chain or kappa light chain. The bound antibodies were detected by the Phototope Western Detection Systems (Cell Signaling Technology, Inc., Danvers, MA).

Epitope Mapping

Epitope mapping studies were performed using the standard Western blotting protocol described above. The NC16A domain of human COL17 was divided into subregions as described by Giudice et al.[15,23] The expression vectors NC16A1, NC16A2, NC16A2.5, and NC16A3, which respectively correspond to amino acid segments 490 to 506, 507 to 520, 514 to 532, and 521 to 534, were gifts from Dr. George J Giudice (Medical College of Wisconsin, Milwaukee). Affinity purified products of recombinant human NC16A and its subregions were electrophoresed and electrotransferred to nitrocellulose membrane. The membranes were then probed with Fabs and allowed to react with HRP-conjugated secondary mAbs to human lambda light chain or kappa light chain.

Immunogold Electron Microscopy

Normal human skin samples were processed for postembedding immunoelectron microscopy as previously described.[24,25] Briefly, cryofixed cryosubstituted samples were embedded in Lowicryl K11M resin and polymerized at −60°C under UV light. Selected blocks were used to produce ultrathin sections that were incubated with Fabs (80 μg/ml), diluted in PBS-based buffer, and washed four times (five minutes each). Further incubations were performed using rabbit anti–c-*myc* tag antibody (Santa Cruz Biotechnology, Santa Cruz, CA) followed by four washes and further incubation with 5-nm gold-conjugated antibody for immunogold labeling (Biocell, Cardiff, UK) diluted 1 in 200 in TBS buffer. Other primary anti-COL17 antibodies included for comparison were HD4 233, 1D1, and 1A8C, each of which recognizes different domains of human COL17 (extracellular domain close to the C-terminal, mid portion, and cytoplasmic domains, respectively).[26] Sections were viewed under a Hitachi H-7100 transmission electron microscope (Hitachi, Tokyo, Japan) at 80 KV.

Immunofluorescence

Five-μm cryosections of OCT-embedded skin were cut and placed onto microscope slides and subjected to IF studies. IIF using Fabs was performed on the skin samples from human or COL17 humanized mice using a standard protocol. FITC conjugated secondary antibodies against human lambda light chain (DakoCytomation, Glostrup, Denmark), kappa light chain (Invitrogen Corp., Carlsbad, CA), or c-*myc* tag (Santa Cruz Biotechnology) were used as detection reagents.

Surface Plasmon Resonance Analysis

Affinity of the generated Fabs was determined by BIAcore assay. The on and off rate constants (k_{on} and k_{off}) for binding of the Fabs to rhNC16A were determined by a BIAcore 2000 instrument (Biacore AB, Uppsala, Sweden). For analysis of the interaction kinetics, Fabs in various concentrations (100, 80, 60, 50, and 40 nmol/L) were injected over the immobilized antigen at a flow rate of 20 μl/min using HBS-EP buffer (Biacore AB). The association and dissociation phase data were fitted simultaneously to a 1:1 Langmuir global model by using the

BIAevaluation software. The affinities (dissociation constant, K_D) were calculated from the ratio of the rate constants of association and disassociation (k_{on}/k_{off}).

Functional Analysis of Fabs in Vitro

Preparation of BP Autoantibodies

BP autoantibodies were purified from either pooled sera from 20 patients or were included as separate serum samples from three patients with active BP. Briefly, the total IgG fraction from BP sera was prepared by affinity chromatography using HiTrap Protein G HP column (Amersham Biosciences UK Limited). Then, BP autantibodies against the COL17 NC16A peptide were affinity purified from the IgG fraction using HiTrap NHS-activated HP column (Amersham Biosciences UK Ltd.) precoated with rhNC16A according to the manufacturer's instructions.[3] The NC16A affinity purified BP autoantibodies were dialyzed against PBS and concentrated by Amicon ultrafiltration (Millipore). These NC16A affinity purified BP autoantibodies were designated as BP antibodies (BPAbs), and used for *in vitro* inhibition experiments.

For the *in vivo* experiments using whole BP-IgG fractions as the pathogenic autoantibodies, serum samples were collected from another 10 BP patients and total IgG fraction was prepared using HiTrap NHS-activated HP column. This was designated as BP-IgG. Binding activity with different autoantigens was tested by ELISA and Western blotting. The BP-IgG from all ten of the serum samples bound to human COL 17, and the BP-IgG from seven of the ten serum samples also reacted with BP230. The binding of the BP-IgG with the subdomains of NC16A (NC16A-1, -2, -2.5, -3, as described by Giudice et al[15]) was further studied. All ten of the serum samples bound to NC16A-2 and NC16A-2.5. In addition, two of the ten serum samples also bound to NC16A-1 or -3. When the pooled IgG from these ten patients was first incubated with the NC16A domain of COL17 overnight at 4°C, the reaction with the NC16A domain was markedly reduced, whereas binding to the full length COL17 was unchanged by Western blotting. This indicates that the BP-IgG recognize numerous epitopes on both COL17 and BP230 antigens, and that there exist autoantibodies recognizing different epitopes both within and outside of the COL17 NC16A domain.

Inhibition ELISA

To check the competition effect of Fabs on the binding of BPAbs to rhNC16A, an inhibition ELISA was performed by incubating purified BPAbs (8 μg/ml) with 0 to 32 μg/ml Fabs on rhNC16A ELISA plates. To detect the IgG autoantibodies, the plates were developed with HRP-conjugated polyclonal antibody to human IgG (DakoCytomation) and o-phenylenediamine substrate. Absorbance was read at 492 nm. The reduced reaction of BPAbs with rhNC16A was expressed as an inhibition rate, which was calculated according to the following formula: inhibition rate % = (A492*b* − A492*f*)/A492*b* × 100, where A492*b* is the reaction with BPAbs only and A492*f* is the reaction competed with Fab at a given concentration.

Inhibition ELISA between phage antibodies (Phabs) and Fabs from the isolated clones was performed to determine whether the Fabs against different epitopes mutually cross-inhibit binding by steric hindrance. Individual Phabs were incubated with rhNC16A on ELISA plates. The reaction was challenged with Fabs from different clones at various concentrations. After washing, the remaining binding of the Phabs to rhNC16A was developed with the HRP-conjugated anti-M13 antibody and o-phenylenediamine substrate.

Inhibition IF

Inhibition IF was assessed to check the competition of Fabs to the binding of BPAbs by incubating purified BPAbs (10 μg/ml) with 0 to 40 μg/ml Fabs on human skin sections. FITC-conjugated anti-human IgG (DakoCytomation) was the detection reagent. The inhibition IF was also performed by sequential incubation with BPAbs on human skin sections, which was followed by Fabs with a 30-minute interval. The effects of Fab inhibition on the binding of autoantibodies from patients with linear IgA bullous dermatosis and anti-p200 pemphigoid were also observed.

In Vitro *Inhibition of BPAb-Induced Complement Activation*

BPAb-induced complement activation in human skin samples and the inhibitory effects of anti-COL17 NC16A Fabs were observed by IF as described by Nelson et al with minor modifications.[9] Cryosections of normal human skin were incubated with BPAbs (10 μg/ml), anti-COL17 NC16A Fabs (10 to 40 μg/ml), or BPAbs plus anti-COL17 NC16A Fabs for one hour at 37°C. Freshly prepared normal human serum was then added as a complete complement source. One hour after incubation, *in situ* deposition of human C1q and C3 at the DEJ was detected with FITC-conjugated mAbs to human C1q and human C3 (DakoCytomation), respectively.

Effects of Fabs on BP Mouse Model in Vivo

All mouse procedures were approved by the Institutional Animal Care and Use Committee of Hokkaido University, and the experimental mice were housed in a specific pathogen-free animal facility. The BP model mice were produced by injecting BP autoantibodies, either NC16A affinity purified BPAbs (50 μg/g body weight) or whole BP-IgG (1 mg/g body weight) prepared from BP patients, into the COL17 humanized neonatal mice, as previously reported.[3] At 48 hours after the injection, the mice developed human BP-like clinical and histological characteristics with serum autoantibody titers ranging from 1:80 to 1:640 in IIF and a mean BP180 antibody index value of 55.7 ± 21.1 by ELISA measurement, which is similar to the autoantibody level usually found in the sera of active BP patients. To observe the effects of the generated

anti-COL17 NC16A Fabs on the COL17 humanized mice and on the BPAb-induced disease, we divided the neonatal mice into different groups. We first injected Fabs from the three individual clones to test whether the recombinant Fabs themselves are pathogenic in COL17 humanized mice. The Fab doses were 30 to 90 μg/g body weight (30 μg/g body weight is roughly an equimolar dose compared with 50 μg/g body weight of IgG-BPAbs). To sequentially monitor the serum Fab levels after injection, 60 μg/g body weight of Fab-B4 was injected into the neonatal mice and blood samples were collected by sacrificing mice at 6, 24, 48, and 72 hours. The Fab concentration was quantified using a sandwich ELISA technique with two mAbs. To capture Fabs in the samples, rabbit anti–c-*myc* mAb (Santa Cruz Biotechnology) was coated onto ELISA plates (20 μg/ml in PBS overnight at 4°C). After blocking with 3% BSA for one hour at 37°C, individual serum samples were diluted with 1% BSA in PBS buffer (1:10) and incubated for 1 hour at 37°C. Purified Fab was used as a standard at concentrations ranging between 0.1 μg/ml and 50 μg/ml. The plate was then incubated with HRP-conjugated mouse anti-human lambda light-chain mAb to detect the reaction. The concentrations of Fabs in the samples were calculated from the standard curve for each plate.

The effects of Fabs on the BP autoantibody-induced mouse model were observed by injecting Fabs either from individual clones or from various combinations of the clones. The injection of antibodies into mice was performed as described previously, with minor modifications.[3] Briefly, each mouse received a single intraperitoneal injection of different antibodies according to group. At 48 hours after injection, the extent of skin disease was judged, including distinct Nikolsky sign. The animals were then sacrificed, and skin samples were studied by light microscopy and direct immunofluorescence microscopy using FITC conjugated antibodies against human lambda light chain (DakoCytomation), c-*myc* tag (Santa Cruz Biotechnology), human IgG (Jackson, West Grove, PA), and mouse complement C3 (Cappel, ICN Pharmaceuticals, Inc., Aurora, OH). The quantification of mast cells (MCs) and MC degranulation was performed as described by Nelson et al, and the results were expressed as a percentage of degranulated MCs (number of degranulated MCs per total number of MCs in 5 random fields × 100%).[9]

Blood was collected, and the serum sample was prepared and used for ELISA to determine the titers of circulating BPAbs or Fabs. The level of BPAbs in the serum samples of experimental mice was tested using an anti-COL17 ELISA kit according to the manufacturer's instructions (MBL, Nagoya, Japan). Absorbance was read at 450 nm. The index value was defined by the following formula: index = (A450 of tested serum − A450 of negative control)/(A450 of positive control − A450 of negative control) × 100. The concentration of the recombinant Fabs in serum samples obtained from the experimental mice was quantified using the sandwich ELISA technique described above.

Statistical Analysis and Ethical Considerations

Differences in the ELISA inhibition results among various groups were examined for statistical significance using the analysis of variance with Fisher PLSD test. For the analysis of MC degranulation among various groups of Fab treatments, we determined statistical significance using multiple tests including the Student *t* test and one way analysis of variance. *P* values less than 0.05 were considered significant.

This study was approved by the Institutional Review Board of Hokkaido University, and fully informed consent from all patients was obtained for use of human material.

Results

Isolation of Anti-COL17 NC16A Antibodies from Phage Antibody Libraries

Two individual Fab phage libraries containing 8×10^7 clones and 4×10^7 clones, respectively, were successfully constructed by combining light chain genes and heavy chain genes amplified from antibody repertoires of two BP patients (library 1 from patient 1; library 2 from

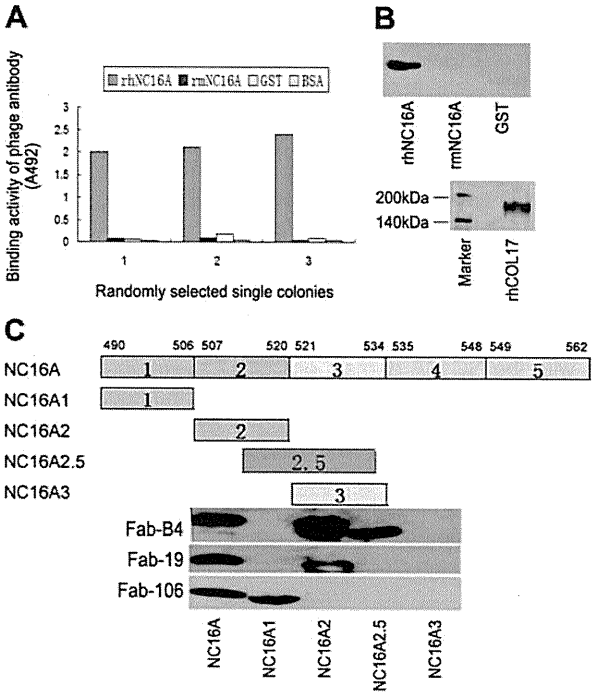

Figure 1. Isolation of specific binders against the NC16A domain of human type XVII collagen from phage antibody library. **A:** Randomly selected single colonies from the fourth panning round of the libraries show positive reaction with recombinant human NC16A (rhNC16A) but no reaction with recombinant mouse NC16A (rmNC16A), GST, or BSA in ELISA. **B:** Western blotting of soluble Fabs shows staining of only the rhNC16A domain and full-length human COL17, whereas rmNC16A and GST are negative. The representative results using Fab-B4 are shown. **C:** Epitope mapping of the generated Fabs with rhNC16A and its subdomains are shown. Fab-B4 binds to rhNC16A, NC16A2, and NC16A2.5 but does not react with NC16A1 and NC16A3, indicating that the binding epitope is located within an overlapping region within subdomain 2 and 2.5 (amino acids 514 to 520). The Fab-106 and Fab-19 epitopes are located in subdomain 1 (NC16A1, amino acids 490 to 506) and subdomain 2 (NC16A2, amino acids 507 to 520), respectively.

Table 2. Heavy and Light Chain Genes of Isolated Fabs

Fab clone	VH family	Amino acid sequences of VH			VL family	Amino acid sequences of VL		
		CDR1	CDR2	CDR3		CDR1	CDR2	CDR3
B4	VH1	NYAFSW	GIIPMSGEGHKAQKFQG	PSRSNYAGGMDV	Vλ1	SGSSSNIGRHYVY	TNYRRPS	ASWDDSL
B12	VH3	SYSMN	SISSSSSYIYYADSVKG	IDSSSWYEGWFDP	Vλ1	SGSTSNIGSNTVN	SNNQRLS	GTWDDSLN
B21	VH3	SYVLS	LLVVMLEADTTQTPEG	GNNWYGQTFDF	Vλ1	GAAPTSGQVMMYTW	GNSNRPS	QSYDSSLS
F32	VH3	SYAMH	VISYDGSNKYYADSVKG	ALRGYSYGT	Vκ1	RASQSISSYLN	AASSLQS	QQSYSLF
19	VH3	NYGMH	VISYDGSKKYYADSVKG	GFYYDWGTYYDY	Vλ1	TGSSSNIGAGYDVH	ANSNRPS	QSYDSSLT
106	VH3	DSAIH	RVRSKTNNYATDYAVSVKGR	HGESRSWYVGSGYWFDP	Vλ1	SGSSSNIGNNYVS	DNNKRPS	GTWDSSLS

Six unique antibody clones against the NC16A domain of human COL17 were identified by sequencing the heavy and light chain variable regions. Of these, clones B4, B12, B21, and F32 were isolated from library 1, whereas clones 19 and 106 were isolated from library 2. The deduced amino acids sequences of the complementary determining regions (CDRs) are shown.

patient 2). Phabs were selected by panning against rhNC16A immobilized on immune tubes. ELISA of the Phabs revealed specific positive reactions with rhNC16A in 40 of 96 and 32 of 80 colonies isolated from the two libraries, respectively (Figure 1A). By BstN I fingerprinting and sequencing of variable regions of heavy chain (VH) and light chain (VL) genes, nine unique antibody clones against rhNC16A were identified and were allowed to express the soluble Fab fragments.

Expression and Characterization of Fabs

Soluble Fab fragments of the nine antibody clones were successfully expressed by removing the gene III fragment of the phagemid vector. Four of the soluble Fabs from library 1 (Fab-B4, Fab-B12, Fab-B21, Fab-F32) and two from library 2 (Fab-19, Fab-106) were highly specific to rhNC16A in ELISA (data not shown) and Western blot analysis (Figure 1B, representative Western blot result). The other three clones, however, could not be detected as soluble fragments, probably because of their low affinity. The VH and VL genes of the six positive Fab clones are summarized in Table 2.

By epitope mapping, the binding site of the Fabs with rhNC16A and its subdomains was obtained. All four of the Fabs from library 1 showed the same reactive pattern. They bound to rhNC16A and subdomains 2 and 2.5 but failed to react with subdomains 1 and 3, indicating that their binding epitope was within the overlapping region (amino acids 514 to 520) of subdomains 2 and 2.5. The two Fabs from library 2 bound to different subdomains: Fab-106 reacted only with subdomain 1 (amino acids 490 to 506) and Fab-19 reacted only with subdomain 2 (amino acids 507 to 520). This indicates that they bound to different epitopes on COL17 NC16A. The representative blot results are shown in Figure 1C. These data demonstrate the successful isolation of anti-COL17 NC16A Fabs from patients with BP.

We chose Fabs (Fab-B4, Fab-19, and Fab-106) that had been raised against different epitopes of COL17 NC16A for further experiments. All of the light chains of these three clones are from human lambda light chain family. Large-scale production was performed, and a yield of approximately 1 to 3 mg of Fab product was obtained from each 1 L culture after column purification. Figure 2A shows the SDS-PAGE identification of the purified Fab in reduced and nonreduced form.

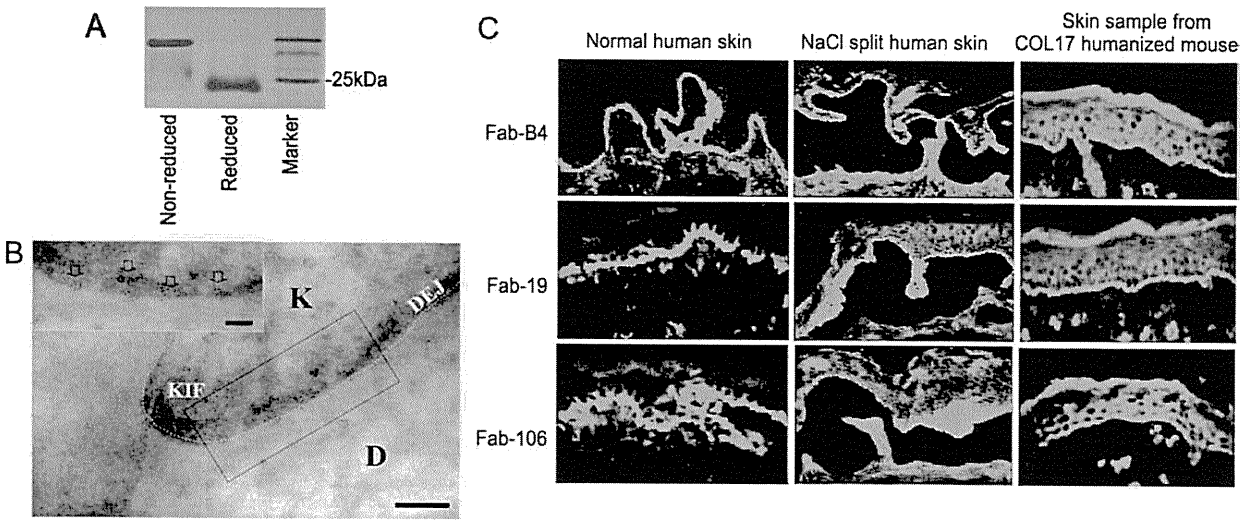

Figure 2. Production and characterization of Fabs. **A:** A purified soluble Fab in both reduced and nonreduced states is shown by Coomassie blue staining after SDS-PAGE. **B:** Immunogold labeling of normal human skin by Fabs shows 5-nm immunogold deposits restricted to immediately beneath hemidesmosomes, close to the keratinocyte plasma membrane (**arrows**, bar = 100 nm). The representative results using Fab-B4 are shown. (**K:** keratinocyte; **D:** dermis; KIF: keratin intermediate filaments; DEJ: dermal-epidermal junction). **C:** Immunofluorescence studies on normal human skin and skin sections from COL17 humanized mice show positive staining of the selected Fabs at the DEJ, and positive staining is also noted on the roof of NaCl split skin samples.

Table 3. Affinity of Anti-COL17 NC16A Fabs Measured by BIAcore System

Fab	k_{on} (1/Ms)	k_{off} (1/s)	K_D (M)
Fab-B4	2.83×10^5	1.10×10^{-3}	3.89×10^{-9}
Fab-19	1.14×10^5	6.26×10^{-3}	5.48×10^{-8}
Fab-106	5.52×10^5	8.08×10^{-2}	1.46×10^{-7}

Kinetic parameters k_{on} and k_{off} were measured by BIAcore system, and K_D was calculated as k_{on}/k_{off}. From the three Fabs, Fab-B4 has the highest affinity.

Immunogold electron microscopy showed that 5-nm immunogold particles were restricted to immediately beneath hemidesmosomes, below the keratinocyte plasma membrane (Figure 2B). Mean measurements of immunogold deposits demonstrated that their epitopes were about 1 to 2 nm (mean 1.77 nm ± SD, $n > 200$) beneath the plasma membrane and located between the epitopes of 1A8C, a cytoplasmic plaque associated COL17 antibody) and 233 (an extracellular COL17 antibody), as described by Nonaka et al.[26] No difference in distribution of the immunogold deposits was found between the three Fabs.

In the IIF experiments, as we expected, all three Fabs showed linear deposition at the DEJ and positive staining was noted along the roof of the NaCl split skin samples, consistent with COL17 staining (Figure 2C).

Kinetic analysis using the BIAcore system demonstrated affinity levels of Fab-B4, Fab-19, and Fab-106, as summarized in Table 3. Among these Fabs, Fab-B4 showed the highest affinity value and Fab-106 showed the lowest.

Functional Analysis of Fabs in Vitro

To determine whether the Fabs generated against COL17 NC16A were able to function in competitive binding to inhibit the emergence of an autoantibody-mediated BP phenotype, we initially performed a series of *in vitro* experiments to evaluate their ability to block BP autoantibody binding to COL17. Figure 3A shows that the rhNC16A binding activities of BPAbs, which were affinity purified using recombinant COL17 NC16A peptide from the pooled sera from 20 BP patients, were reduced markedly and significantly by Fab-B4 and Fab-19, but only marginally by Fab-106, in a dose-dependent manner (0 to 32 μg/ml). Fab-B4 and 19 suppressed the binding of BPAbs most efficiently at a concentration of 32 μg/ml, with the highest inhibition rates of 52.4% and 50.8%, respectively. Combinations of two or three Fabs failed to increase this inhibition efficacy. When tested with BPAbs isolated from individual BP patients, Fabs showed similar competitive effects (Figure 3B).

IIF studies show competitive blocking of Fabs with BPAbs on skin sections. Figure 4 shows positive IgG

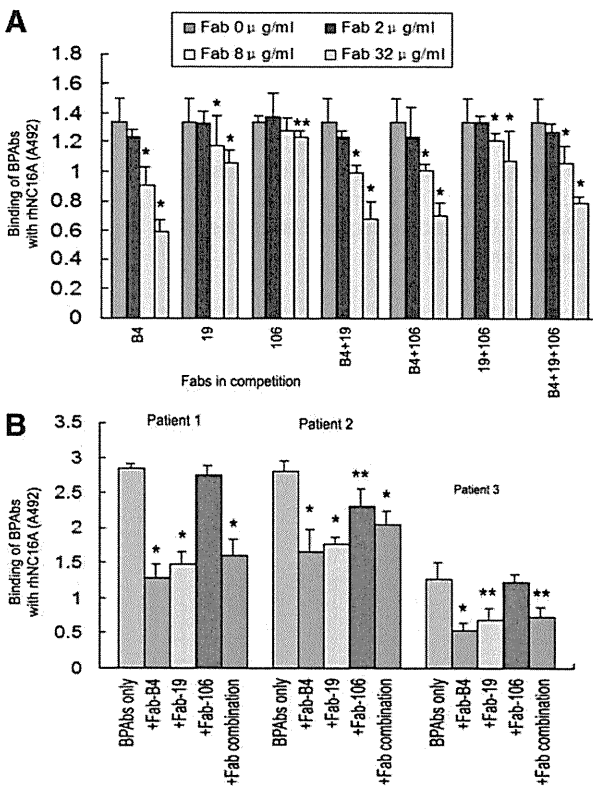

Figure 3. Inhibition ELISA assay. **A:** The effects of competition with Fab-B4, Fab-19, and various combinations inhibit the binding of autoantibodies (BPAbs, 8 μg/ml) from pooled sera of patients with bullous pemphigoid (BP) to rhNC16A in a dose-dependent manner (0 to 32 μg/ml), whereas Fab-106 inhibits BPAb binding only moderately. $^*P < 0.01$, $^{**}P < 0.05$, versus the original binding of BPAbs. **B:** Fabs (32 μg/ml) inhibit the binding of BPAbs from three BP patients. $^*P < 0.01$, $^{**}P < 0.05$, versus the original binding of BPAbs.

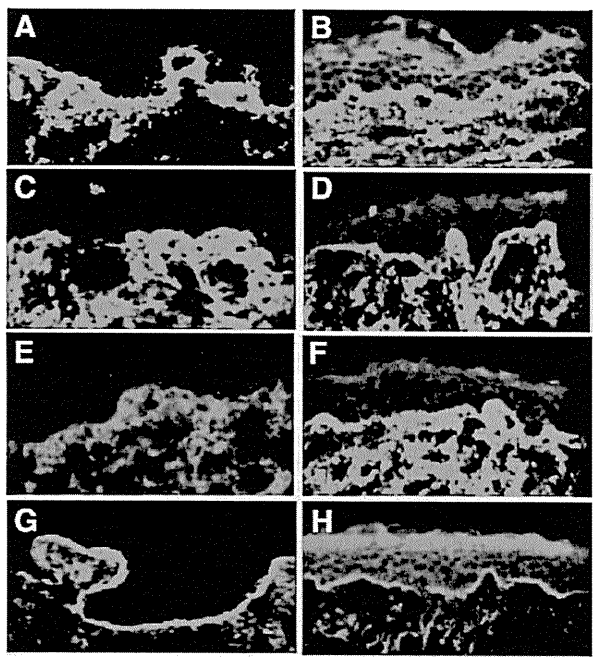

Figure 4. Inhibition immunofluorescence. **A** and **B:** Positive IgG staining of the NC16A affinity purified BPAbs (10 μg/ml) at the DEJ in human skin. **C** and **E:** IgG BPAbs staining is blocked by coincubation with either Fab-B4 or Fab-19 at a concentration of 20 μg/ml. **G:** Fab-106 (20 μg/ml) fails to significantly inhibit the binding of BPAbs. When BPAbs are allowed to bind to skin sections first and Fabs are added 30 minutes later, the IF staining of BPAb binding is also markedly reduced by Fab-B4 (**D**) or Fab-19 (**F**) but not by Fab-106 (**H**).

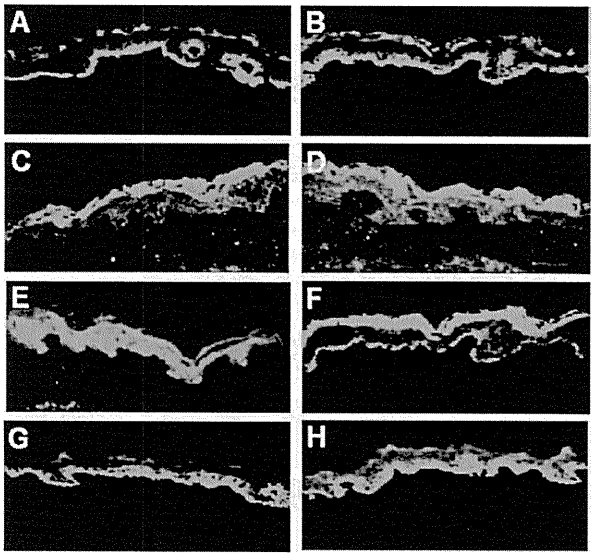

Figure 5. BPAb-induced complement activation and the inhibitory effects of Fabs. NC16A affinity purified BPAbs (10 μg/ml) induced activation of human C1q and C3 is shown at the DEJ in cryosections of human skin (**A** and **B**). When Fabs are coadministered with BPAbs at the same concentration, Fab-B4 completely blocks C1q and C3 activation (**C** and **D**), whereas Fab-19 effectively blocks the activation of C1q (**E**) and markedly reduces the activation of C3 (**F**). Fab-106 shows no inhibition of either C1q or C3 activation (**G** and **H**).

BPAbs staining (10 μg/ml) at the DEJ in human skin (Figure 4A), which was blocked by coincubation with either Fab-B4 or Fab-19 at a concentration of 20 μg/ml (Figure 4, C and E). Fab-106 failed to significantly inhibit the binding of BPAbs (Figure 4G). When BPAbs were allowed to bind to skin sections first and Fabs were added 30 minutes later, the IF staining of BPAb binding was also markedly reduced although not completely inhibited (Figure 4, B, D, F, and H). Competitive IF using Fabs and individual patient BPAbs showed that Fab-B4 and Fab-19 were able to block the binding of autoantibodies from three individual BP patients, whereas none of the Fabs inhibited the binding of IgA autoantibodies from patients with linear IgA bullous dermatosis or IgG autoantibodies from patients with anti-p200 pemphigoid (data not shown).

In vitro inhibition of complement activation by recombinant Fabs was studied by immunofluorescence. *In situ* deposition of BPAb-activated C1q (Figure 5A) and C3 (Figure 5B) was found at the DEJ in human skin. Complement deposition was reduced or completely blocked by Fab-B4 (Figure 5, C and D) or Fab-19 (Figure 5, E and F), whereas it was unchanged by Fab-106 treatment (Figure 5, G and H). Fabs against COL17 NC16A did not activate complement at concentrations up to 100 μg/ml.

We also tested the effect of competition between recombinant anti-COL17 NC16A Fabs. Using an inhibition ELISA, Fabs from the three clones inhibited the binding of Phabs from their own clone as we might have expected. Interestingly, Fab-B4 and Fab-19 cross-inhibited each other while Fab-106 failed to inhibit the other two (Figure 6, A–C). These data indicate that Fab-B4 and Fab-19 specifically recognize distinct but close or overlapping

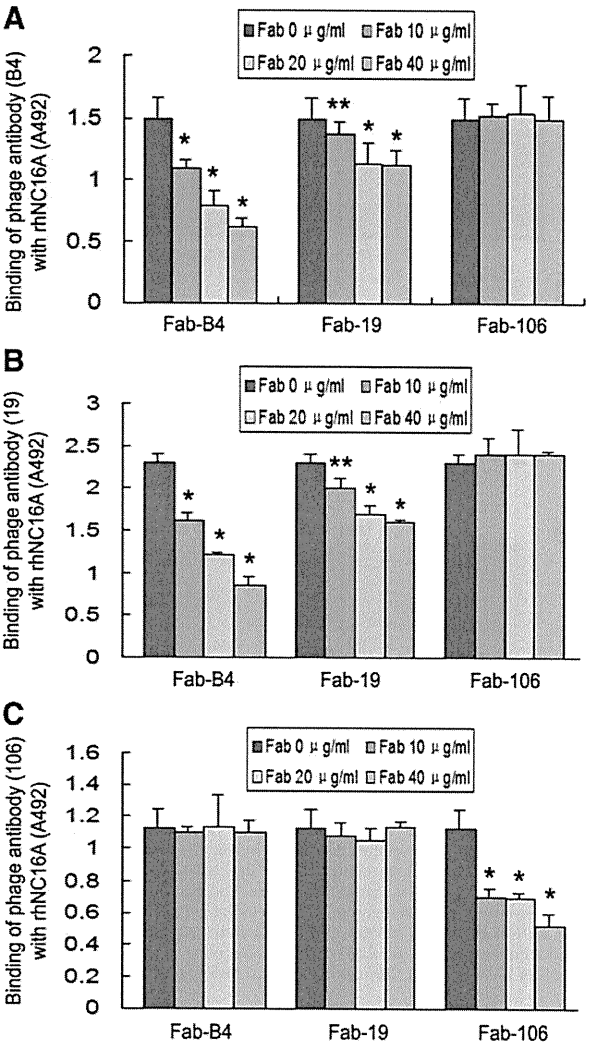

Figure 6. Inhibition ELISA for the three recombinant antibody clones using Fabs and phage antibodies (Phabs). Fab-B4 and Fab-19 inhibited the binding of both Phab-B4 and Phab-19 (**A** and **B**), whereas Fab-106 inhibited Phab-106 only (**C**). This indicates that the antibody clones B4 and 19 are mutually cross-inhibiting. $^{*}P < 0.01$, $^{**}P < 0.05$, versus the original binding of respective Phabs.

epitopes and are able to block the binding of BP antibodies in nearby epitopes, most likely by direct steric hindrance.

In Vivo *Blockade of Autoantibody-Induced BP Disease*

We first proved that recombinant Fabs were not pathogenic to COL17 humanized mice after injection with 30 to 90 μg/g body weight of Fab-B4, -19, or -106 into neonatal mice. Neither clinical signs, including erythema and Nikolsky sign, nor any histopathological manifestations of BP were found in the treated mice. Direct immunofluorescence studies demonstrated clear deposition of the recombinant Fab fragments at the DEJ. Subsequent deposition of mouse C3 was not detected (Figure 7A).

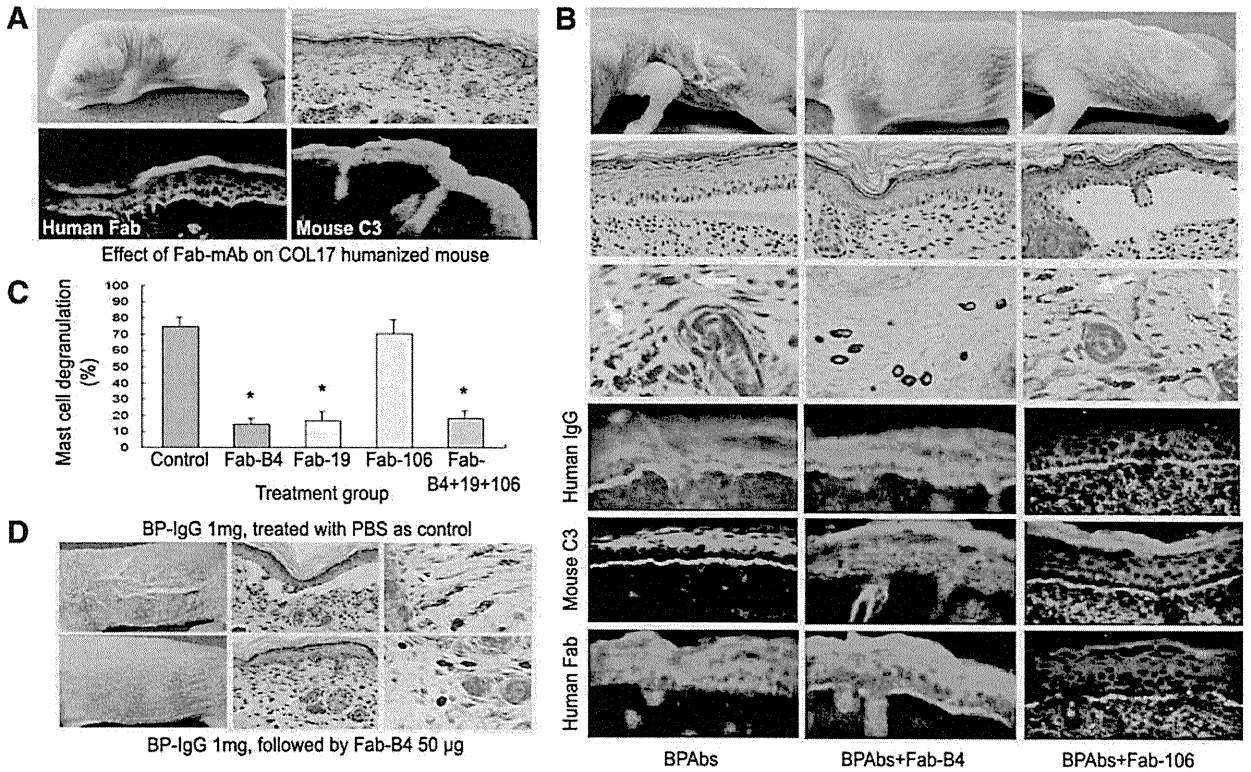

Figure 7. Therapeutic effects of Fabs on BP model mice. **A:** Results of the injection of Fabs into neonatal COL17 humanized mice show that this treatment alone does not cause BP disease or other detectable adverse effects. Histological examination (**right, upper panel**) supports this result. Indirect immunofluorescence show DEJ staining for the recombinant Fabs (**left** of **lower panel**) but no staining for mouse C3 (**right, lower panel**). **B:** Mice injected with NC16A affinity purified BPAbs develop the clinical and histological skin detachment associated with MC degranulation (**white arrows**) and the deposition of human IgG and mouse C3 at the DEJ. In contrast, mice injected with BPAbs and Fab-B4 fail to show these clinical and histological characteristics, and the intensity of IgG deposition at the DEJ is markedly reduced. The staining of mouse C3 is absent, whereas recombinant Fab fragment staining is weak but detectable. Fab-106 fails to show any beneficial therapeutic effect in the animal model. **C:** Percentage of dermal MC degranulation is assessed in BP model mice and in those treated with 30 μg/g body weight of Fabs. It is significantly reduced in the mice treated with Fab-B4, Fab-19, and the Fab combination. $^{*}P < 0.01$ versus control group (BP model mice treated with PBS). **D:** BP model mice were produced by injection of BP-IgG (total IgG fraction prepared from BP patients) and were treated with Fab-B4 24 hours later. BP-like clinical and histological characteristics fail to develop in most (four of five) of Fab-B4 treated mice (**lower panel**).

For further *in vivo* experiments, we again used the humanized BP mouse model and induced disease by injecting BP autoantibodies, either BPAbs (50 μg/g body weight) or whole BP-IgG (1 mg/g body weight), into neonatal COL17 humanized mice. We sequentially analyzed the serum concentration of BP autoantibodies in the injected mice. Their autoantibody titers ranged from 1:80 to 1:640 in IIF, and the mean BP180 antibody index value reached the highest level of 72.8 ± 21.7 at 6 hours and then gradually decreased to 68.5 ± 9.1 at 12 hours, 64.1 ± 14.9 at 24 hours, 55.7 ± 21.1 at 48 hours, 33.4 ± 4.8 at 72 hours, and 33.7 ± 2.6 at 96 hours after injection. After i.p. injection of BPAbs or whole BP-IgG, the mice were i.p. treated either immediately or 24 hours later with Fabs from each of the three individual clones. The results were evaluated 48 hours later (Table 4). As shown in Figure 7B, the BP model mice untreated with Fabs demonstrated a BP-like clinical phenotype with extensive erythema and Nikolsky sign together with histological characteristics, including dermal-epidermal separation and the infiltration of inflammatory cells. These clinical and histological signs failed to develop in any of the Fab-B4 groups, including the immediately treated and the 24 hour–treated mice. Treatment with Fab-19 demonstrated a similar effect. Fab-106, however, failed to show any therapeutic efficacy. Histologically, no subepidermal blister formation was found in skin samples from mice treated with Fab-B4 or -19 at a dosage of 30 μg/g body weight or higher, whereas distinctive BP-like blister formation was observed in skin sections from the majority of the Fab-106 treated mice (4/5 mice with the 30 μg/g body weight treatment and 4/4 mice with the 60 μg/g body weight treatment) or control mice. Fab combination therapy at the same total dose showed a similar result as treatment with Fab-B4 or -19 alone. Direct immunofluorescence studies revealed that deposition of human IgG and mouse C3 at the DEJ was significantly reduced in the Fab-B4 or -19 treated groups compared with that of controls. Extensive MC degranulation took place in the dermis of the BP model mice. In contrast, the percentage of degranulated MCs was significantly decreased in the Fab-B4– and -19–treated mice (Figure 7C). Figure 7D shows the BP disease phenotype induced by injection of whole BP-IgG (upper panel) and the therapeutic results of Fab (lower panel). Fab-B4 treatment inhibited the BP-IgG–induced phenotypic changes in all immediately treated mice, as well as the majority of the mice (4/5) treated 24 hours after the initial BP-IgG injection. To-

Table 4. Effects of Anti-COL17 NC16A Fabs on BP Autoantibody-Induced Mouse Model

Abs used for reproducing mouse model	Treatment	Total dose of Fab (μg/g body weight)	Skin detachment
COL17 NC16A- affinity purified BP autoantibodies (BPAbs)	Fab-B4	15	2/8
		30	0/10
		30 (24 hours later)	0/4
		60	0/9
	Fab-19	15	2/6
		30	0/6
		60	0/6
	Fab-106	15	5/5
		30	4/5
		60	4/4
	Fab combination (Fab-B4 + 19 + 106)	15	2/5
		30	0/6
		60	0/5
	Control	PBS	14/14
Whole IgG fractions (BP-IgG)	Fab-B4	30	0/4
		30 (24 hours later)	1/5
	Control	PBS	4/4

Neonatal COL17 humanized BP model mice were injected with either COL17 NC16A-affinity purified BP autoantibodies (BPAbs: 50 μg/g body weight) or whole IgG fractions (BP-IgG: 1 mg/g body weight) from patients with bullous pemphigoid. The mice were then treated immediately or 24 hours later (underlined) with Fabs by intraperitoneal injection. For Fab combination therapy, the total dose comprised one third of each Fab clone.

gether with the *in vitro* inhibition IF data, these results demonstrate that Fabs can at least partially displace the bound BP autoantibodies within the DEJ and block BP disease after initial binding not only by NC16A-purified BPAbs but also by combined whole IgG sera fractions from BP patients. When the mice were sacrificed at 48 hours, serum samples were collected to detect BP antibody index values and the recombinant Fab level. The BP180 antibody index value in the control mice sera was 170.3 ± 26.2, and no significant increase or decrease was found in any of the treatment groups ($P > 0.05$). The concentrations of Fabs ranged from 1.34 ± 0.11 μg/ml to 10.22 ± 0.35 μg/ml, increasing with increasing injected dose; however, there was no significant difference between the mice injected with Fabs only and the BP model mice treated with Fabs at the same given doses ($P > 0.05$). No adverse reactions to the Fab treatments were observed.

Discussion

In the present study, we successfully generated Fabs against the human COL17 NC16A domain from phage display antibody repertoires derived from two BP patients. These Fabs specifically recognize different epitopes located in NC16A subdomains and competitively inhibit the binding of human BP autoantibodies to COL17. Our novel anti-COL17 NC16A Fabs were observed to inhibit the changes in the BP mouse model that would otherwise have been induced by the injection of human BP autoantibodies into recently engineered COL17-humanized mice.

BP is the most common autoimmune blistering skin disease. The mortality rate of BP in various reports ranges from 20% to 40%, and death is more commonly related to other underlying illness, debilitation associated with severe BP condition, or adverse effects of treatment.[27] Autoantibodies against two hemidesmosomal antigens, BPAG1 (BP230) and BPAG2 (COL17 or BP180), have been identified in BP. COL17 autoantibodies are generally thought to play a critical role in the initial pathogenesis of the disease. COL17, a type II transmembrane protein, is the main pathogenic target for BP autoantibodies and the NC16A domain was subsequently confirmed as the main binding epitope.[15,28–30] COL17 autoantibodies have been widely studied and have been shown to induce activation of complement via a classical pathway that is essential for disease development. This allowed us to devise a new approach toward treating BP and a therapeutic strategy for such treatment. Using molecular and recombinant protein techniques, we identified three Fabs, Fab-B4, Fab-19, and Fab-106, which recognize multiple epitopes within the COL17 NC16A domain with different affinity levels. Of these, Fab-B4 and Fab-19 recognized distinct epitopes located within subdomain 2 of NC16A, whereas Fab-106 recognized an epitope in subdomain 1. Interestingly, Fab-B4 and Fab-19 inhibited each other in competition ELISA assays using reciprocal Phabs and soluble Fabs, indicating that they bind specifically to their corresponding epitopes and may involve mutual steric hindrance. Fab-106 showed no inhibitory effects on the other two Fabs, confirming its unique binding domain.

Fab-B4 and Fab-19, but not Fab-106, showed therapeutic potential for BP in both *in vitro* and *in vivo* studies. Both fragments competitively inhibit the binding of BP autoantibodies to the main COL17 NC16A epitope, and both of them block BPAb-mediated activation of complement C1q and C3. In our BP animal model using the COL17 humanized mouse, marked inhibition of the BP phenotype, including deposition of BPAbs and complement, degranulation of MCs, and subcutaneous blister formation, was observed in Fab-B4– or Fab-19–treated mice. It appears from these data that complete blocking of BP autoantibodies by Fabs is not required to significantly inhibit disease severity. We know this because

successful treatment of the BP model mouse was achieved even with partial blocking of BP autoantibody binding. This is consistent with the clinical observation that BP symptoms can markedly improve as the autoantibody levels gradually decrease, although autoantibodies are still detectable.[31,32] This suggests that there may be a threshold for BP autoantibodies to initiate and maintain complement activation and complement-mediated tissue injury. Partially reducing autoantibody deposition using blocking Fabs might be beneficial in alleviating BP. Furthermore, our Fab was demonstrated to be able to displace the bound BP autoantibodies both *in vitro* and *in vivo*. These results strongly support our approach of using inhibitory anti-COL17 NC16A Fabs for BP therapy. When comparing the *in vitro* and *in vivo* activities of all these Fabs together, the Fab-B4 clone appears to be most efficient. We assessed the effects of combining these three Fabs, but we failed to improve on the results. The inhibitory effect of Fab clones in combination was not as good as that of the Fab-B4 clone alone, even at equivalent dosages. The administration of Fabs themselves or in combination failed to elicit any adverse pathological manifestation in the COL17 humanized mice.

It has been shown that the majority of anti-COL17 autoantibody pathogenic epitopes are mainly distributed in subdomains 1 to 3 of NC16A.[33] Fairley et al[23] further defined subdomain 2 as the major epitope recognized by both IgG and IgE autoantibodies from BP patients. We tested the reactivity of BP autoantibodies and found that the binding amount and affinity against subdomain 2 was higher than the binding amount and affinity for subdomains 1 and 3 (data not shown). Taken together with the fact that anti-subdomain 2 Fabs show excellent therapeutic effects in BP model mice, even after the disease was induced not only by the COL17 NC16A affinity purified BPAbs, but also by whole BP-IgG fractions, we speculate that the BP autoantibodies that recognize the non-NC16A epitopes may be less pathogenic than those that recognize the NC16A epitopes. The BP autoantibodies that recognize NC16A, especially the subdomain 2 region, are the main pathogenic autoantibodies in BP. Previously reported *in vitro* studies using cryosections[34] and *in vivo* animal models[10] both suggested that anti NC16A autoantibodies are major pathogenic antibodies in BP, which further supports our speculation.

Thus far, the complement system has been an attractive therapeutic target for a wide range of autoimmune and inflammatory diseases.[2,13] There are different strategies of inhibiting complement activation. In a previous study, we tried using a recombinant peptide containing BP pathogenic epitopes as a decoy to block both the binding of BP autoantibodies and the activation of complement.[3] Although it proved effective, a potential pitfall exists. The peptide may act as an antigen and trigger a more severe immune response, and hence, result in further production of pathogenic autoantibodies. Fab therapy eliminates such concerns. Furthermore, it is highly disease-specific and does not involve systemic immune suppression; therefore, it may be used either as an individual therapy or in combination with other currently available treatments to promote efficacy and reduce adverse reactions. Our success in generating these Fabs with therapeutic potential makes it possible to create not only a more specific therapy for BP but also further potential strategies for the treatment of many other antibody-initiated complement-mediated autoimmune disorders.

Acknowledgments

We thank Ms. Noriko Ikeda, Ms. Maki Goto, Ms. Megumi Sato, and Ms. Akari Nagasaki for their technical assistance.

References

1. Jacobson DL, Gange SJ, Rose NR, Graham NM: Epidemiology and estimated population burden of selected autoimmune diseases in the United States. Clin Immunol Immunopathol 1997, 84:223–243
2. Holers VM: The complement system as a therapeutic target in autoimmunity. Clin Immunol 2003,107:140–151
3. Nishie W, Sawamura D, Goto M, Ito K, Shibaki A, McMillan JR, Sakai K, Nakamura H, Olasz E, Yancey KB, Akiyama M, Shimizu H: Humanization of autoantigen. Nat Med 2007, 13:378–383
4. Liu Z, Giudice GJ, Swartz SJ, Fairley JA, Till GO, Troy JL, Diaz LA: The role of complement in experimental bullous pemphigoid. J Clin Invest 1995, 95:1539–1544
5. Mewar D, Wilson AG: Autoantibodies in rheumatoid arthritis: a review. Biomed Pharmacother 2006, 60:648–655
6. D'Cruz DP, Khamashta MA, Hughes GRV: Systemic lupus erythematosus. Lancet 2007, 369:587–596
7. Girardi G, Berman J, Redecha P, Spruce L, Thurman JM, Kraus D, Hollmann TJ, Casali P, Caroll MC, Wetsel RA, Lambris JD, Holers VM, Salmon JE: Complement C5a receptors and neutrophils mediate fetal injury in the antiphospholipid syndrome. J Clin Invest 2003, 112:1644–1654
8. Zhao M, Trimbeger ME, Li N, Diaz LA, Shapiro SD, Liu Z: Role of FcRs in animal model of autoimmune bullous pemphigoid. J Immunol 2006, 177:3398–3405
9. Nelson KC, Zhao M, Schroeder PR, Li N, Wetse RA, Diaz LA, Liu Z: Role of different pathways of the complement cascade in experimental bullous pemphigoid. J Clin Invest 2006, 116:2892–2900
10. Liu Z, Diaz LA, Troy JL, Taylor AF, Emery DJ, Fairley JA, Giudice GJ: A passive transfer model of the organ-specific autoimmune disease, bullous pemphigoid, using antibodies generated against the hemidesmosomal antigen BP180. J Clin Invest 1993, 92:2480–2488
11. Liu Z: Bullous Pemphigoid: Using animal models to study the immunopathology. J Investig Dermatol Symp Proc 2004, 9:41–46
12. Yancey KB: The pathophysiology of autoimmune blistering diseases. J Clin Invest 2005, 115:825–828
13. Girardi G, Redecha P, Salmon JE: Heparin prevents antiphospholipid antibody-induced fetal loss by inhibiting complement activation. Nat Med 2004, 10:1222–1226
14. Atkinson JP: Complement system on the attack in autoimmunity. J Clin Invest 2003, 112:1639–1641
15. Giudice GJ, Emery DJ, Zelickson BD, Anhalt GJ, Liu Z, Diaz LA: Bullous pemphigoid and herpes gestationis autoantibodies recognize a common non-collagenous site on the BP180 ectodomain. J Immunol 1993, 151:5742–5750
16. Wang Z, Wang Y, Li Z, Li J, Dong Z: Humanization of a mouse monoclonal antibody neutralizing TNF-α by guided selection. J Immunol Methods 2000, 241:171–184
17. Barbas III CF, Kang AS, Lerner RA, Benkovic SJ: Assembly of combinatorial antibody libraries on phage surfaces: The gene III site. Proc Natl Acad Sci USA 1991, 88:7978–7982
18. Little M, Breitling F, Dubel S, Fuchs P, Braunagel M: Human antibody libraries in Escherichia coli. J Biotechnol 1995, 41:187–195
19. Clackson T, Hoogenboom HR, Griffiths AD, Winter G: Making antibody fragments using phage display libraries. Nature 1991, 352: 624–628
20. Wang G, Liu YF, Li CY, Lu N, Gao TW, Hua B, Wang Y: Cloning and

characterization of antikeratin human antibodies using a semisynthetic phage antibody library. Arch Dermatol Res 2004, 296:270–277
21. Marks JD, Hoogenboom HR, Bonnert TP, McCafferty J, Griffiths AD, Winter G: Bypassing immunization of human antibodies from V-gene libraries displayed on phage. J Mol Biol 1991, 222:581–597
22. Hoogenboom HR: Selecting and screening recombinant antibody libraries. Nat Biotechnol 2005, 23:1105–1116
23. Fairley JA, Fu CL, Giudice GJ: Mapping the binding sites of anti-BP180 immunoglobulin E autoantibodies in bullous pemphigoid. J Invest Dermatol 2005, 125:467–472
24. Shimizu H, Masunaga T, Ishiko A, Hashimoto T, Garrod DR, Shida H, Nishikawa T: Demonstration of desmosomal antigens by electron microscopy using cryofixed and cryosubstituted skin with silver-enhanced gold probe. J Histochem Cytochem 1994, 42:687–692
25. McMillan JR, Akiyama M, Nakamura H, Shimizu H: Colocalization of multiple laminin isoforms predominantly beneath hemidesmosomes in the upper lamina densa of the epidermal basement membrane. J Histochem Cytochem 2006, 54:109–111
26. Nonaka S, Ishiko A, Masunaga T, Akiyama M, Owaribe K, Shimizu H, Nishikawa T: The extracellular domain of BPAG2 has a loop structure in the carboxy terminal flexible tail in vivo. J Invest Dermatol 2000, 115:889–892
27. Khumalo N, Kirtschig G, Middleton P, Hollis S, Wojnarowska F, Murrell D: Interventions for bullous pemphigoid. Cochrane Database Syst Rev 2005 (3):CD002292
28. Schumann H, Baetge J, Tasanen K, Wojnarowska F, Schäcke H, Zillikens D, Bruckner-Tuderman L: The shed ectodomain of collagen XVII/BP180 is targeted by autoantibodies in different blistering skin diseases. Am J Pathol 2000, 156:685–695
29. Ishiko A, Shimizu H, Kikuchi A, Ebihara T, Hashimoto T, Nishikawa T: Human autoantibodies against the 230-kD bullous pemphigoid antigen (BPAG1) bind only to the intracellular domain of the hemidesmosome, whereas those against the 180-kD bullous pemphigoid antigen (BPAG2) bind along the plasma membrane of the hemidesmosome in normal human and swine skin. J Clin Invest 1993, 91:1608–1615
30. Stanley JR: Autoantibodies against adhesion molecules and structures in blistering skin diseases. J Exp Med 1995, 181:1–4
31. Kobayashi M, Amagai M, Kuroda-Kinoshita K, Hashimoto T, Shirakata Y, Hashimoto K, Nishikawa T: BP180 ELISA using bacterial recombinant NC16a protein as a diagnostic and monitoring tool for bullous pemphigoid. J Dermatol Sci 2002, 30:224–232
32. Tsuji-Abe Y, Akiyama M, Yamanaka Y, Kikuchi T, Sato-Matsumura KC, Shimizu H: Correlation of clinical severity and ELISA indices for the NC16A domain of BP180 measured using BP180 ELISA kit in bullous pemphigoid. J Dermatol Sci 2005, 37:145–149
33. Zillikens D, Rose PA, Balding SD, Liu Z, Olague-Marchan M, Diaz LA, Giudice GJ: Tight clustering of extracellular BP180 epitopes recognized by bullous pemphigoid autoantibodies. J Invest Dermatol 1997, 109:573–579
34. Sitaru C, Schmidt E, Petermann S, Munteanu LS, Brocker EB, ZIllikens D: Autoantibodies to bullous pemphigoid antigen 180 induce dermal-epidermal separation in cryosections of human skin. J Invest Dermatol 2002, 118:664–671

ORIGINAL ARTICLE

A study of Zinc Contained in Yellow and Black Discolored Nails by X-ray Fluorescence and X-ray Absorption Fine Structure Analyses

Motohiro UO[1], Kiyotaka ASAKURA[2], Erika WATANABE[3], Inkin HAYASHI[3], Teruki YANAGI[3], Hiroshi SHIMIZU[3], and Fumio WATARI[1]

[1] Department of Biomedical Materials and Engineering, Graduate School of Dental Medicine, [2] Catalyst Research Center, [3] Department of Dermatology, Graduate School of Medicine, Hokkaido University, Sapporo, Japan

Synopsis

The elements in discolored nails were assessed by X-ray fluorescence analysis (XRF), and the chemical state of Zn in the nail samples was assessed by X-ray absorption fine structure (XAFS) analysis. Compared to the normal nail, a part of the yellow nail contained a considerably high amount of Ca, whereas the black nail contained higher amounts of Ca and Zn. The chemical state of Zn in the yellow nail was similar to that in the normal nail. The Zn in the black nail was in a slightly different chemical state, suggesting the existence of different chemical species of Zn in the black nail.

Key words: *nail, zinc, elemental analysis, X-ray absorption fine structure (XAFS)*

Introduction

The nail is a keratinous skin appendage that contains a high concentration of cysteine residues. The nail plate also contains minerals such as magnesium (Mg), calcium (Ca), iron (Fe), and zinc (Zn) [1]. The shape and color of the nail reflects the systemic health conditions, and black, yellow, green, or white discoloration of the nails is seen clinically [2]. Black nail reportedly occurs because of an increase in nail matrix melanocytes, an infectious pathology, malignant melanoma, etc [2-4]. Yellow nail syndrome is caused by nutritional deficiency, respiratory manifestations, infection of nails, and jaundice [2, 5].

Zn is one of the main minerals in the nail plate. The content of Zn in nails is higher in males than in females, and is related to nail discoloration and its treatment. One of the causes of black discoloration of nails is the production of the black mineral sulfide from the hydrogen sulfide derived from the microbes causing infections [3]. Arroyo et al. reported that oral zinc supplementation with ZnS improved the discolored nail [6]. These minerals have the possibility of the nano particle combined with nail proteins. Therefore, analysis of the concentration and chemical state of Zn is important to determine the causes of nail discoloration.

In this study, the elemental minerals in the yellow and black nails were assessed by performing X-ray fluorescence (XRF) analysis. In

addition, the chemical states of Zn in these nail samples were estimated by performing X-ray absorption fine structure (XAFS) analysis.

Materials and Methods

1. Specimens

Yellow discolored nails were obtained from a 71-year-old man, and black discolored nails were obtained from a 54-year-old man. The yellow nails consisted of 2 parts: a slightly yellow part (A) and a considerably yellow part (B). In addition, normal nail specimens were collected from a healthy volunteer for reference purpose. These specimens were applied to the following analyses.

2. XRF analysis

The elements in the nail specimens were assessed by using a fluorescence X-ray spectrometer (XGT-2000V; Horiba Co. Ltd., Kyoto, Japan). Incident X-rays generated from an Rh anode under conditions of 50 kV and 1 mA were irradiated into the center of the specimens through an X-ray guide tube (XGT) having a diameter of 100 μm. The analysis time for each specimen was 1,200 sec. The composition of the detectable elements (S, K, Ca, Fe, and Zn) was quantitated by using the fundamental parameter method (standardless method) [7].

3. XAFS analysis

The XAFS spectra were measured at beamline 12C in the Photon Factory at the High Energy Accelerator Research Organization (KEK-PF). The electron storage ring was operated at 2.5 GeV with 450 mA. Synchrotron radiation was monochromatized with a Si(111) double-crystal monochromator. The incident X-ray was focused on an area of 1 mm in diameter by using two bent conical mirrors, and the specified areas of the specimens were irradiated. The Zn K-edge X-ray absorption near-edge structure (XANES) spectra of the specimens were measured using the fluorescent XAFS method with a 19-elements solid-state detector (SSD; Camberra, Meriden, U.S.A.). The I_0 signals were monitored using an N_2-filled ionization chamber. The metallothionein that contains Zn and Cd (Sigma-Aldrich, St.Louis, U.S.A.) was also subjected to XRF and XAFS analyses as the reference of Zn contained in a metalloprotein. The XANES spectra of reference materials (Zn foil, ZnO, and ZnS) were measured using a ordinary transmission method.

Results and Discussions

The fluorescence X-ray spectra of the normal, black, and yellow discolored nails are shown in Fig. 1. The elemental composition estimated using the standardless method is presented in Table 1. XRF analysis cannot detect the light elements (e.g., H, C, N, and O); hence, the elemental composition in Table 1 shows the weight ratio of the 5 detected elements. The normal nail had a very strong peak assigned to sulfur (S), which was derived from the keratin of the nail. In addition, clear peaks derived from K, Ca, Fe, and Zn were also observed. The S content was higher than 80wt%, and Ca, K and Fe concentrations were also measured. Zn was clearly detected, but its content was less than 1wt%. The Ca:S ratio was approximately 0.1, and the Zn:S ratio was quite low (0.008). Thus, the normal and healthy nail consists of keratin and small amount of minerals. The slightly yellow nail (A) showed an elemental composition similar to the normal nail,

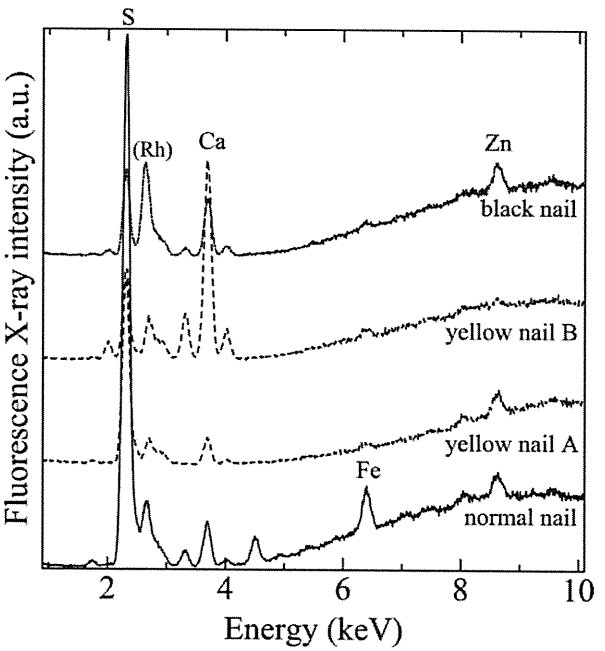

Fig.1 XRF spectra of the normal, yellow, and black nails

Table 1 Element composition of nail specimens (wt%).

Elements	Normal	Yellow (A)	Yellow (B)	Black
S	84.5	81.7	23.4	48.3
K	4.4	0.4	12.6	6.3
Ca	8.6	15.6	62.7	40.8
Fe	1.8	0.6	0.9	1.2
Zn	0.7	1.7	0.4	3.4
Ca:S	0.10	0.19	2.7	0.84
Zn:S	0.008	0.02	0.017	0.070
Ca:Zn	13	9.0	170	12

but the considerably yellow nail (B) showed an extremely strong Ca peak. The Ca:S ratio of the considerably yellow nail (B) was 2.7; this value is quite higher than that of the normal nail (0.10), suggesting the presence of a large amount of calcified matter in this nail type. In contrast, the Zn content in this considerably yellow nail was about half of that in the normal nail. The black nail showed a clear Zn peak, and the Zn content was found to be 5 times higher than that in the normal nail. Karita et al. have reported the Ca, Mg, and Zn levels in fingernails [8]: the Ca:Zn ratio was reported to be 0.6~28.4 (median = 5.7). In our study, the yellow nail (B) showed a Ca:Zn ratio of more than 170, which is much higher than that reported by Karita et al. In case of the black nail, the Ca:Zn ratio was in the normal range, but the Zn:S ratio (0.07) was higher than that in the other nail specimens, indicating that the Zn content was quite higher than the S (keratin) in the black nail.

Fig. 2 shows the Zn k-edge XANES spectra of the normal, yellow, and black nails. The XANES spectrum of the normal nail showed a good resemblance to that of metallothionein, which is a type of cysteine-rich protein that can bind to heavy metals such as Zn, Cu, and Cd through a thiol group of cysteine residues. Metallothionein is suggested to play a role in the detoxification of heavy metals and regulation of essential trace metal elements. Thus, Zn in the nail possibly exists as a protein complex, similar to metallothionein. The yellow nail showed a XANES spectrum that was quite similar to that of the normal nail, then the chemical state of Zn in the yellow and normal nails would be similar. The edge energy of the black nail was the same as that of the other nails; however, the shape of the spectrum was slightly different from the other spectra and it showed a small peak at around 9666eV. This result suggested that existence of different chemical species in the black nail. One of the causes of the black nail reported by Zuehlke et al. is the production of hydrogen sulfide by microbes when they react with the metallic elements in the nail and consequently produce black metal sulfides [3]. The XANES

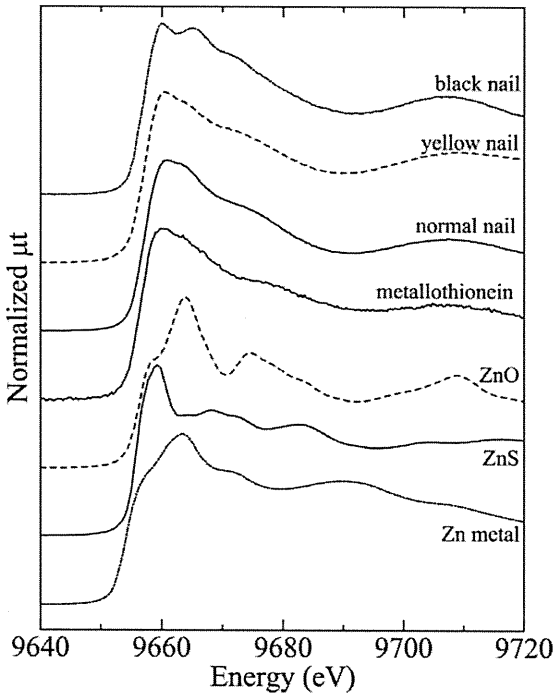

Fig.2 Zn K-edge XANES spectra of the normal, yellow, and black nails